

**EFFECTS OF PROCESSING PARAMETERS ON PRODUCTION OF
GRAPHENE BY MECHANICAL EXFOLIATION**

MUHAMAD ZARIF BIN ANUAR

**BACHELOR OF CHEMICAL ENGINEERING
UNIVERSITI MALAYSIA PAHANG**

**EFFECTS OF PROCESSING PARAMETERS ON PRODUCTION OF
GRAPHENE BY MECHANICAL EXFOLIATION**

MUHAMAD ZARIF BIN ANUAR

Thesis submitted in partial fulfilment of the requirements
for the award of the degree of
Bachelor of Chemical Engineering

**Faculty of Chemical & Natural Resources Engineering
UNIVERSITI MALAYSIA PAHANG**

2017

UNIVERSITI MALAYSIA PAHANG

DECLARATION OF THESIS AND COPY RIGHT

Author's Full Name : Muhamad Zarif Bin Anuar

Date of Birth : 22 February 1994

Title Effect of Processing Parameters on Production of
Graphene by Mechanical Exfoliation

Academic Session : Semester 2 2016/2017

I declared that this thesis is classified as:

CONFIDENTIAL (Contains confidential information under the Official Secret Act 1972)*

RESTRICTED (Contains restriction information as specified by the organization where research was done)*

OPEN ACCESS I agree that my thesis to be published as online open access (Full text)

I acknowledge that University Malaysia Pahang reserve the right as follows:

1. The Thesis is the Property of University Malaysia Pahang.
2. The Library of University Malaysia Pahang has right to make copies for the purpose of research only.
3. The Library has the right to make copies of the thesis for academic exchange.

Certified By:

(Student's Signature)

(Supervisor's Signature)

New IC /Passport Number
Date:

Name of Supervisor
Date:

NOTES : *If the thesis is **CONFIDENTIAL** or **RESTRICTED**, please attach with the letter from the organization with period and reasons for confidentiality or restriction

SUPERVISOR'S DECLARATION

We hereby declare that we have checked this thesis and in our opinion, this thesis is adequate in terms of scope and quality for the award of the degree of Bachelor of Chemical Engineering.

Signature :
Name of main supervisor : Dr. Kamal Bin Yusoh
Position : SENIOR LECTURER
Date :

STUDENT'S DECLARATION

I hereby declare that the work in this thesis is my own except for quotations and summaries which have been duly acknowledged. The thesis has not been accepted for any degree and is not concurrently submitted for award of other degree

Signature :

Name : Muhamad Zarif Bin Anuar

ID Number : KA14154

Date :

Dedicated to my father, and my mother.

ACKNOWLEDGEMENT

I would like to express my special appreciation and thanks to my supervisor, Dr. Kamal Bin Yusoh. You have been a brilliant mentor for me. I would like to thank you for your never ending support during my tenure as research student under your guidance, for giving insightful comments and suggestions of which without it, my research path would be a difficult one . Your advice on my research has been valuable.

My fullest appreciation goes as well to Mr. Abu Haniffa Bin Abdullah and Ms. Fadwa Sameha Binti Ismail, for their idea and support from the beginning till the end of my research.

A special thanks to my family. Words cannot express how grateful I am to my mother, father, for the love and support throughout these years. Your prayer for me was what sustained me thus far.

I would also like to thank all of my friends who supported me in writing, and motivate me to strive towards my goal. I am sincerely grateful to the staffs of Chemical Engineering and Natural Resources Faculty who helped me in financial support through research grant. Many thanks go to staff at Central Lab, Carrif Lab, FIST Lab as well as FKKSA Lab of University of Malaysia Pahang for assisting me in testing my sample.

ABSTRACT

Graphene, a monolayer form of carbon with two dimensional honeycomb lattices (sp² Hybridization) has shown excellent mechanical, electrical, thermal and optical properties. It is a promising component for many applications in the fields of electronics, composites, sensors as well as energy storage and conversion devices. These engineering applications require availability of graphene on the mass scale and thus suitable processes are necessary for its production down to few sheets level. In the present work, the objective is to study the effect of processing parameter on preparation of graphene at large scale by liquid phase exfoliation of graphite assisted by ultra sound to promote the intercalation and expansion of graphite by using homogenizer. Water and tea polyphenol was choose and act as a dispersion agent and antioxidant. From the result, it is found that the graphene dispersion concentration is increased when the sonication time and power increased with the highest concentration of 1.0699 mg/ml. But, by controlling the centrifuged speed, the result shows no influenced on dispersion concentration. In Addition, the size of the sheets also become smaller when increasing sonication time and power. However, from the XRD analysis, it can be conclude that the graphite only partially exfoliated with the stack of several or tens of single layer graphite. Therefore, by controlling LPE critical parameter likes sonication power, sonication time and centrifuged speed, graphene can produce at high scale.

ABSTRAK

Grafen ialah lapisan yang satu molekul tebal yang terdiri daripada karbon atom yang berbentuk 2-dimensi heksagon (sp^2 penghibridan) dan mempunyai sifat-sifat mekanik, elektrik, terma dan optik yang sangat baik. Ia merupakan komponen yang berpotensi untuk banyak bidang aplikasi seperti elektronik, komposit, sensor dan penyimpanan tenaga dan juga peranti penukaran. Oleh itu, ia memerlukan aplikasi kejuruteraan yang bersesuaian untuk memproses grafen pada skala yang besar sambil mengekalkan kualiti pada tahap yang tinggi. Penyelidikan ini bertujuan untuk membuat kajian terhadap kesan parameter pemrosesan dalam menghasilkan grafen pada kuantiti yang banyak dengan menggunakan kaedah pengelupasan grafit yang menggunakan tenaga ultrasonik untuk menggalakkan interkalasi dan pengembangan grafit dengan menggunakan alat homogenizer. Air dan *tea polyphenol* dipilih sebagai ejen penyebaran dan juga berfungsi sebagai antioksidan. Hasilnya, kepekatan penyebaran grafen meningkat apabila durasi dan kuasa ultrasonik meningkat dengan jumlah tertinggi iaitu 1.0699 mg/ml. Tetapi, apabila mengawal kelajuan emparan, dilihat tidak memberi kesan pada kepekatan penyebaran grafen. Tambahan pula, saiz lembaran juga dilihat mengencil apabila durasi dan kuasa ultrasonik meningkat. Walau bagaimanapun, grafit tidak dapat mencapai pengelupasan yang lengkap seperti mana dapat dilihat di XRD analisa. Oleh itu, dengan mengawal parameter penting seperti kelajuan emparan, kuasa dan durasi ultrasonik, grafen dapat dihasilkan dalam kuantiti yang banyak.

TABLE OF CONTENTS

	Page
SUPERVISOR’S DECLARATION	ii
STUDENT’S DECLARATION	iii
ACKNOWLEDGEMENT	v
ABSTRACT	vi
ABSTRAK	vii
TABLE OF CONTENTS	vii
LIST OF TABLES	x
LIST OF FIGURES	xi
LIST OF SYMBOLS	xiii
LIST OF ABBREVIATIONS	xiv
CHAPTER 1 INTRODUCTION	1
1.1 Background of the Study	1
1.2 Motivation	2
1.3 Problem Statement	2
1.4 Objectives	3
1.5 Scopes of Study	3
CHAPTER 2 LITERATURE REVIEW	4
2.1 Properties of Graphene	4
2.2 Application of Graphene and its Derivatives.	6
2.3 Synthesis of Graphene	8
2.3.1 Micromechanical Exfoliation of Graphene	8
2.3.2 Reduction of Graphene Oxide	8
2.3.3 Chemical Vapor Deposition of Graphitic on Metallic Substrate	9
2.3.4 Mechanical Assisted Liquid Phase Exfoliation of Graphite into Graphene	11
2.4 Effect of Processing Parameters	13
2.4.1 Time	13
2.4.2 Temperature	14
2.4.3 Sonication power	15
2.4.4 Centrifuged Speed	16
2.4.5 Solvent	17
2.4.6 Pressure	18
2.5 Graphene Characterization Tools	19
2.5.1 Raman Spectroscopy Analysis	19
2.5.2 AFM Analysis	21
2.5.3 XRD Analysis	22

2.5.4	UV-VIS Analysis	23
2.5.5	FESEM Analysis	24
2.5.6	TEM Analysis.	24
2.5.7	FTIR Analysis	26
2.5.8	Structure of Thesis	27
CHAPTER 3 METHODOLOGY		28
3.1	Materials	28
3.2	Graphene preparation	28
3.3	Characterization techniques	30
3.3.1	XRD	30
3.3.2	UV-Vis	30
3.3.3	FTIR	30
3.3.4	TEM	30
3.4	Process flow diagram	31
CHAPTER 4 RESULTS AND DISCUSSION		32
4.1	Ultraviolet-Visible Spectroscopy (UV-vis) analysis	32
4.1.1	Concentration of Graphene dispersion	32
4.1.2	Concentration as function of sonication power and centrifuge speed	35
4.1.3	Concentration as function of sonication time	40
4.2	FTIR analysis	43
4.3	TEM Analysis	47
4.4	XRD Analysis	56
CHAPTER 5 CONCLUSION AND RECOMMENDATION		62
5.1	Conclusion	62
5.2	Recommendation	63
REFERENCES		64
Appendix		73

LIST OF TABLES

Table No.	Title	Page
Table 2.1:	The applications of Graphene in different fields.	7
Table 3.1:	Graphite properties	28
Table 3.2:	Summary of experiment sample	29
Table 4.4.1:	Graphene concentration over sonication power and centrifuge speed	35
Table 4.4.2:	Graphene concentration over sonication time	40
Table 4.3:	Peak list summary for samples at different sonication time	59
Table 4.4:	Peak list summary for samples at different sonication power	61

LIST OF FIGURES

Figure No.	Title	Page
Figure 2.1:	Graphite structure	4
Figure 2.2:	Perspective 3D drawing of the graphene lattice structure.	5
Figure 2.3:	Electronic band structure of single-layer graphene	6
Figure 2.4:	Micromechanical exfoliation of HOPG to produce graphene flakes:	8
Figure 2.5:	Schematic of the roll-based production of graphene films grown on a copper foil.	10
Figure 2.6:	Schematic representation of the liquid-phase exfoliation process of graphite in the absence (top-right) and presence (bottom-right) of surfactant.	12
Figure 2.7:	Raman spectra of the graphene grown at different growing time with (a) 15:1 (H ₂ : CH ₄) and (b) 15:1 (H ₂ : C ₂ H ₄) of gas mixing ratio at 950 °C.	14
Figure 2.8:	Length of size selected flakes plotted as a function of final centrifugation rate. Flakes found after final centrifugation at 3000 rpm (small flake) and 5000 rpm (large flakes).	16
Figure 2.9:	Energy level diagram show the states involved in Raman signal	20
Figure 2.10:	A schematic representation of the AFM	21
Figure 2.11:	Schematic principle of operation of the XRD	23
Figure 2.12:	General layout of a TEM describing the path of electron beam in a TEM and a ray diagram for the diffraction mechanism in TEM.	25
Figure 2.13:	Illustrates how the FTIR instrument works.	26
Figure 4.1:	Absorption per unit length as a function of C _g .	33
Figure 4.2:	Graphite flake added to the ultrapure water-tea solution	34
Figure 4.3:	Picture of homogenizer used.	34
Figure 4.4:	Picture of graphene dispersion	34
Figure 4.5:	Schematic diagram of chemical exfoliation method which illustrate the effect of centrifuge.	37
Figure 4.6:	UV-Vis spectra of graphene suspensions at different sonication power (%) and centrifuge speed (rpm)	39
Figure 4.7:	Graphene dispersion at different sonication time in ultra-pure water-tea solution. From left: 1 hour, 3 hour, 5 hour sonication time.	41
Figure 4.8:	UV-Vis spectra of graphene suspensions at different sonication time	42

Figure 4.9: FTIR spectrum of samples at different sonication time.	44
Figure 4.10: FTIR spectrum at different sonication power and centrifuge rate	46
Figure 4.11: TEM image of graphene sheet deposited from 1 hr sonication time sample (scale: 100nm). Yellow arrows show the folded regions.	48
Figure 4.12: TEM images for 2 hr sonication time sample. The graphene particle present in agglomerated form with multiple layers (scale: 100nm).	49
Figure 4.13: TEM image for 5 hr sonication time (scale: 50nm). Partially exfoliated graphite with the stack of several single layer graphite (graphene).	51
Figure 4.14: TEM image for 5 hr sonication time (scale: 100nm). Monolayer and very large sheet can be observed.	52
Figure 4.15: TEM images for sample (a) 40% sonication power (b) 50% sonication power (both image were taken at 9.6k x resolution).	55
Figure 4.16: XRD pattern of graphite sonicated at different time (hr).	58
Figure 4.17: XRD pattern of graphite sonicated at different power (%).	61

LIST OF SYMBOLS

<i>2D</i>	<i>Two-dimensional</i>
<i>g</i>	<i>gram</i>
<i>m</i>	<i>meter</i>
<i>rpm</i>	<i>rotation per minute</i>
<i>W</i>	<i>watt</i>

LIST OF ABBREVIATIONS

AFM	Atomic Force Microscopy
CNT	Carbon Nanotube
CVD	Chemical Vapour Deposition
DMF	Dimethyl Formamide
EG	Expanded Graphite
FET	Field Effect Transistor
FESEM	Field Emission Scanning Electron Microscope
FTIR	Fourier Transform Infrared Spectroscopy
GICs	Graphite Intercalation Compounds
GO	Graphene Oxide
HOMO	Highest Occupied Molecular Orbital
HOPG	Highly-Oriented Pyrolytic Graphite
JCD	Jet Cavitation Device
LED	Light Emitting Diode
LPE	Liquid-phase Exfoliation
LUMO	Lowest Unoccupied Molecular
NMP	N-methyl-pyrrolidinone
PECVD	Plasma Enhanced Chemical Vapor Deposition
PET	Polyethylene terephthalate
PMMA	polymethyl methacrylate
rGO	Reduced Graphene Oxide
SBS	Sedimentation-based Separation
SEM	Scanning Electron Microscope
TEM	Transmission Electron Microscopy

UV-VIS Ultraviolet-visible Spectroscopy

XRD X-ray Powder Diffraction

CHAPTER 1

INTRODUCTION

1.1 Background of the Study

Graphene, the well-publicised and now famous two-dimensional carbon allotrope, is as versatile a material as any discovered on Earth. Its amazing properties as the lightest and strongest material, compared with its ability to conduct heat and electricity better than anything else, mean that it can be integrated into a huge number of applications and because of that it has been intensely studied (Liang et al., 2015). As for electric property, monolayer graphene is semi-metallic and its carrier is massless Dirac Fermions whose dynamics should be described by Dirac equation (Novoselov et al., 2004). The maximum current density which monolayer graphene can bear is several million times larger than that in copper (Moser et al., 2007). Initially this will mean that graphene is used to help improve the performance and efficiency of current materials and substances, but in the future it will also be developed in conjunction with other two-dimensional (2D) crystals to create some even more amazing compounds to suit an even wider range of application.

One of the greatest challenges being faced today in commercializing graphene is how to produce high quality material, on a large scale, and in a reproducible manner. According to Hernandez's group, sonication assisted liquid-phase exfoliation (LPE) of graphite to give graphene has made the large-scale production of graphene possible (Hernandez et al., 2008). Following their experiment in dispersing carbon nanotube by sonication. In their work, graphite powder was dispersed in a specific solvent, followed by sonication and centrifugation. Then graphene dispersion was freeze dried to obtain a graphene powder before being analysed using characterization technique like XRD, Raman spectroscopy, SEM, FESEM, FTIR, UV-VIS, and TEM.

After this work, based on the same idea, many researches have contributed to achieving high concentration and quality of graphene by prolonging the sonication time, increasing the initial graphite concentration, adding surfactants and polymer, solvent exchange method, mixing solvents, etc (Min Yi and Zhigang Shen, 2013).

1.2 Motivation

For the wide and viable applications, high-scale production and availability of graphene are prerequisite. Exfoliation of graphite by sonication to produce graphene can be considered as a suitable approach to accomplished large-scale production. Development on the related theories and design call for scalable, efficient, and controllable production of graphene are still remain top priority.

1.3 Problem Statement

Up to now, a large number of methods have been proposed to produce graphene and majority of them suffer a common problem – to produce at high scale. Graphene production by mechanical exfoliation can be categorized into two major classes, bottom-up and top-down method. Bottom-up technique such as chemical vapour deposition (CVD) and epitaxial growth, can yield graphene with high quality and small number of defects. However, these techniques suffer from the limited scale and expensive production, therefore cannot meet the requirement of large quantities of graphene (Min Yi and Zhigang Shen, 2013). Initially, the standard procedure to make graphene is by micromechanical cleavage. This give the best sample to date, with carrier mobilities up to $200 \text{ cm}^2\text{V}^{-1}\text{s}^{-1}$ (Bolotin et al., 2008). But this method is extremely time-consuming and labour-intensive. Due to this factor, it is limited to the lab scale only and seems impossible to be scaled up to industrial production.

Top-down approaches like sonication assisted LPE is most promising route to accomplished industrial size production. Recently, dispersion and exfoliation of graphene oxide (GO) is a method that have been proposed and discussed in many novel material. GO is material consists of graphene-like sheets, chemical functionalized with compound such as hydroxyls, which stabilize the sheets in water (Stankovich et al., 2007). However,

this functionalization disrupts the electronic structure of graphene. Although it can be removed through reduction, but doing so it will result in leaving a significant number of defects, which continue to disrupt the electronic properties (Eda et al., 2008). Thus, by using a dispersion agent like polyphenol which is a type of antioxidant like tea leaf to produce a significant quantity of defect-free, high scale and unoxidized graphene is urgently required. Furthermore, this antioxidant is non-toxic and environmentally friendly.

1.4 Objectives

The following is the objective of this research:

To study the parameters that affect the scale-up process in the production of graphene by mechanical exfoliation via ultrasonic.

1.5 Scopes of Study

The following are the scope of this research:

- 1) To study the difference in kind of parameter such as sonication time, power, as well as centrifuge speed that affected the scale-up process.
- 2) To upscale the production of graphene based on mechanical exfoliation via sonication from 1g to 500g.
- 3) To identify and confirm the graphene produced using UV-Vis and to characterize based on configuration, orientation, structure as well as functional group by using XRD, TEM, and FTIR method analysis.

CHAPTER 2

LITERATURE REVIEW

2.1 Properties of Graphene

Graphite is combination of millions of the graphene layers. Two type of bond are exist and formed among the graphene layer. The bond which holds together the graphene layers by the weak force are called Vander Waal attraction. Due to this weak strength that hold the layer together, it can slide to each other layer and the attraction is strong enough to do the complete exfoliation into individual layers. On the other hand, the Covalent bond which are present between the carbon-carbon atoms in each layer and can be considered as strong bond. In a simple word, hypothetically, properties of graphene are mainly dependent on their geometric structures.

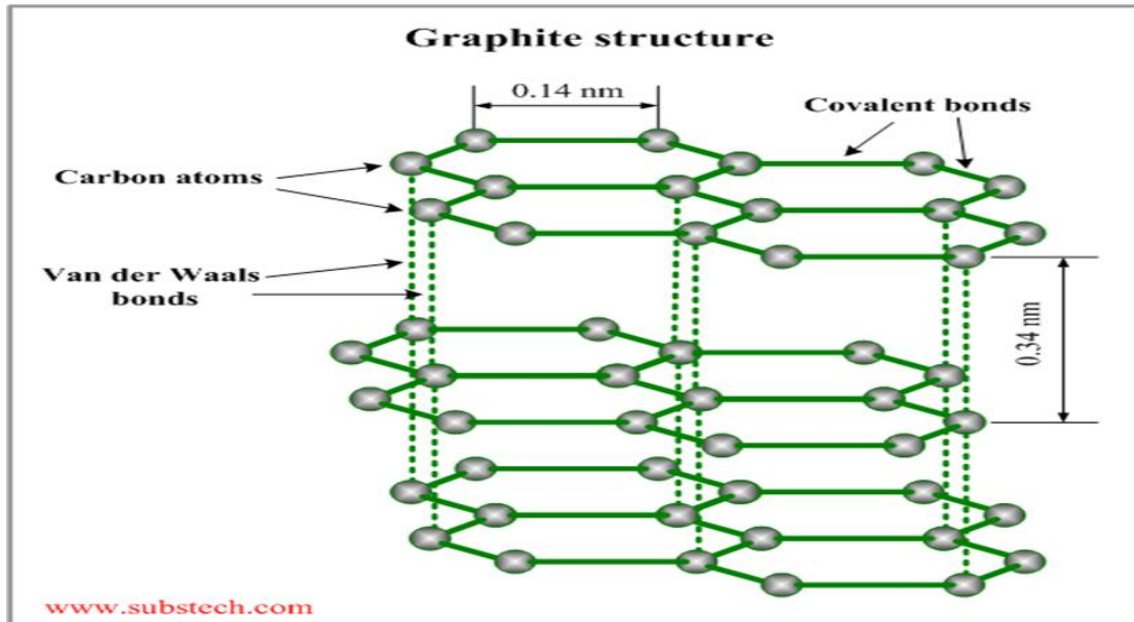


Figure 2.1: Graphite structure

Graphene is a nearly transparent, two-dimensional semimetal consisting of a single atomic lattice of hexagonally arranged sp^2 hybridized carbon atoms (Ruoff, 2008). The quantum mechanical basis proposed to explain the band structure and electronic

behaviour of graphite was first carried out by Wallace in 1947 using the tight binding approximation (Wallace, 1947). He managed to develop the description of the single hexagonal unit cell crystal structure of graphite and corresponding k-space Brillion zone. The tight binding method approximates the Hamiltonian operator for a crystal lattice as the Hamiltonian operator of a single atom within that lattice. In addition, the electron is assumed to be well localized about a given atomic site such that the wave function readily decays outside the range of the lattice constant of the crystal. As a result, the wave functions of electrons moving through the crystal are approximated as the atomic orbitals of their corresponding atoms and there are no other electron interactions within the structure (Ashcroft & Mermin, 1976). Using the tight binding approximation, Wallace was able to qualitatively describe the band structure of the graphitic unit cell which explained some of the observed conductivity behaviour in graphite crystals (Wallace, 1947). However, it was not for another half century that the modelled single layer graphite crystal would be successfully isolated and available to the scientific community. In 2004 single layer graphite, given the name graphene, was isolated and the electronic structure measured by, Andre Geim and Konstantin Novoselov (Novoselov et al., 2004). This work has since ignited substantial research in graphene across many fields of science and engineering on the extraordinary two-dimensional material and earned Geim and Novoselov the 2010 Nobel Prize in Physics.

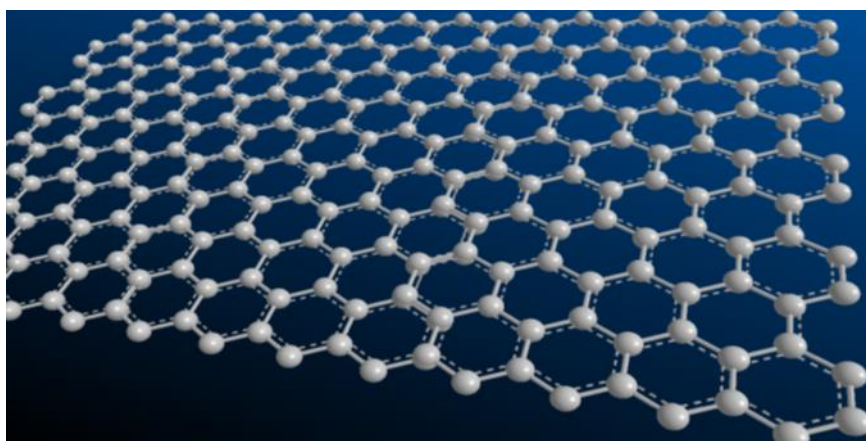


Figure 2.2: Perspective 3D drawing of the graphene lattice structure.

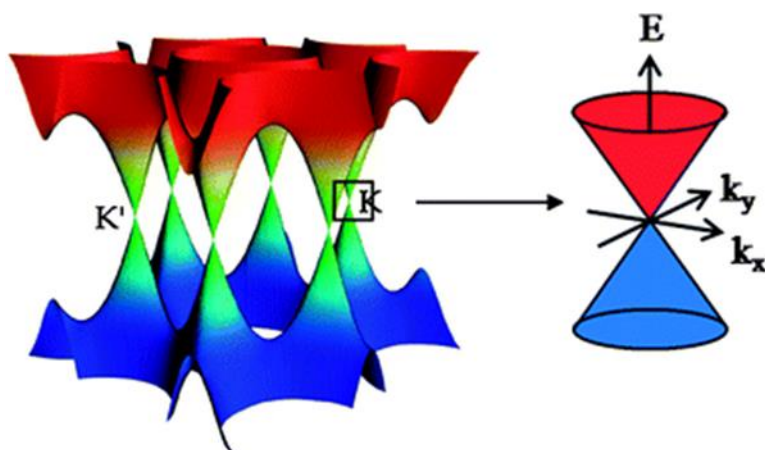


Figure 2.3: Electronic band structure of single-layer graphene

2.2 Application of Graphene and its Derivatives.

The advancement of new-found nanomaterials provides a fascinating opportunity for development in different fields because of their structures, components and properties. In comparison with its precursor, carbon nanotube (CNT), graphene exhibits some merits like low cost, two external surfaces, facile fabrication and modification and absence of toxic metal particles (Liu et al., 2008). Thus graphene and its derivatives are expected to find applications in many fields such as Nano-electronic devices, chemical and biological sensors, energy storage and biomedical fields which have been summarized in Table 2.1.

Because of high electrical conductivity and mechanical flexibility, graphene and its derivatives have got wide spread applications in light emitting diode (LED), field effect transistor (FET), memory and photovoltaic devices. Graphene materials have also been used in fuel cells, solar cells and has been identified as a catalyst support for oxygen reduction and methanol oxidation in case of a fuel cell configuration (Xu et al., 2008). Besides that, Conductive graphene scaffolds for platinum nanoparticles also can facilitates efficient collections as well as transfer of electrons to electrode surface.

However, graphene does not only limited in electronic devices, it also has it own application in biomedical. Dikin et al. demonstrated that GO sheets dispersed in water can assembled into a well ordered structure under a directional flow, yielding ultra-strong GO or rGO paper (Dikin et al, 2007). This graphene paper was used for culturing mouse

fibroblast cell line (L929) and the results confirmed graphene as a good candidate for adhesion and proliferation of L929 cells. Therefore, graphene is also a suitable material for Tissue Engineering.

Table 2.1: The applications of Graphene in different fields.

	Application	
	Graphene	Electronic Nanodevices
Transparent Conductive Films		
Energy Storage Devices		Li-Ion Batteries
		Ultra-Capacitors
		Fuel Cell and Solar Cells
Sensors		Electrochemical Sensors
		Biosensors
Biomedical Engineering		Gene Delivery
		Drug Delivery
		Tissue Engineering
		Cancer Therapy

2.3 Synthesis of Graphene

2.3.1 Micromechanical Exfoliation of Graphene

The work carried out by Geim and Novosolov in 2004 was a simple exfoliation method in which protrusions of highly-oriented pyrolytic graphite (HOPG) were embedded in photoresist and adhesive tape was used to successively peel off layers of graphene (Novoselov et al., 2004). Although tedious, low yield and not industrially scalable, this so called scotch tape method is simple and does not require any modification to environmental parameters such as temperature and pressure. In addition this method provides high quality (high mobility and low defect) single and few layer graphene sheets with large areas as high as $100\mu\text{m}^2$. Figure 2.4 displays a common experimental setup for micromechanical exfoliation (also referred to as micromechanical cleavage).



Figure 2.4: Micromechanical exfoliation of HOPG to produce graphene flakes:

2.3.2 Reduction of Graphene Oxide

The oxidation of graphite into graphene oxide (GO) by use of strong acids is a common method for forming stable solutions of GO dispersed in water (Lee et al., 2012), which can be subsequently reduced either by aqueous reduction agents such as hydrazine (Li et al., 2008) or by thermal reduction under a reducing atmosphere (Pu et al., 2012). The most common procedure for synthesis of GO was developed by Hummer in 1958 and was

based on an improvement from previous experimental methods which were time consuming and dangerous (Hummers & Offeman, 1958). Hummers' method uses a strongly oxidizing solution of sodium nitrate, potassium permanganate and concentrated sulfuric acid to oxidize the basal plane of graphite with carboxylate, hydroxyl, epoxy and carbonyl groups (Ruoff & Park, 2009). Recent experimental improvements on the synthesis of GO have been achieved by the Tour et al which uses a solution of phosphoric and sulfuric acid and potassium permanganate while removing the need for sodium nitrate which eliminates the formation of toxic gases in Hummers method and exhibits higher yields of GO (Marcano et al., 2010).

Solution processing of GO is challenging because GO have high solubility in water due to its polar oxygen functionality. Electronic devices made by the directed self-assembly of continuous GO films on a patterned 3-aminopropyl triethoxy silane (APTES) substrate has been successfully demonstrated by exploiting the net negative charge that GO exhibits and incorporating a positive charge on the silicon substrate by APTES functionalization (Chu, 2012). However, the defects in the graphene crystal structure incurred during the oxidation process irreparably compromise the electronic structure of pristine graphene and reduced graphene oxide (rGO) only exhibits a fraction of the electron mobility, thermal conductivity, and mechanical strength compared to that of pristine graphene.

The successful deposition of non-oxidized graphene from solution onto a substrate in a manner analogous to the work by Chu would enable facile device fabrication and be a major breakthrough for the application of solution based graphene for electronic device fabrication.

2.3.3 Chemical Vapor Deposition of Graphitic on Metallic Substrate

Graphene growth by chemical vapor deposition (CVD) is typically carried out under ultra-high vacuum and at high temperatures (Choi et al., 2010) in which a volatile or gas phase carbon precursor is flowed over a metallic substrate which acts as a catalyst and nucleation site for graphene growth. Graphene produced by CVD was first reported in work by Somani et al in 2006 using nickel foil and camphor for the metallic substrate and

carbon precursor respectively (Somani et al., 2006). In addition to successful multilayer graphene growth on nickel substrates (Yu et al., 2008), analogous methods have grown single layer graphene copper foil substrates. However these methods require high vacuum, in the milli-Torr range, as well as high temperatures in the range of 1000 – 1035°C (Li et al., 2009). Various other carbon precursors have also been shown to successfully grow graphene both in the gas phase such as methane or solids, such as polymethyl methacrylate (PMMA) on a copper foil (Tan et al., 2011). Work by the Tour et al has also shown that graphene on a copper substrate can be grown from virtually any solid carbon containing source (Ruan et al., 2011).

The graphene produced by CVD is more transferable to various substrates compared to epitaxial graphene, but does require chemical etching of the metallic substrate. Polyethylene terephthalate (PET) supported large area graphene screens have been demonstrated by Bae et al which exhibited relatively high carrier mobility of $5,100 \text{ cm}^2 \text{ V}^{-1} \text{ S}^{-1}$ a 90% optical transparency and sheet resistance of $30 \text{ } \Omega/\text{sq}$ compared to the industrially common transparent conductor indium tin-oxide (ITO) which exhibits 90% transparency and a $100 \text{ } \Omega/\text{sq}$ sheet resistance (Bae et al., 2010). Wafer scale CVD graphene has also been fabricated for thin film transistor devices.

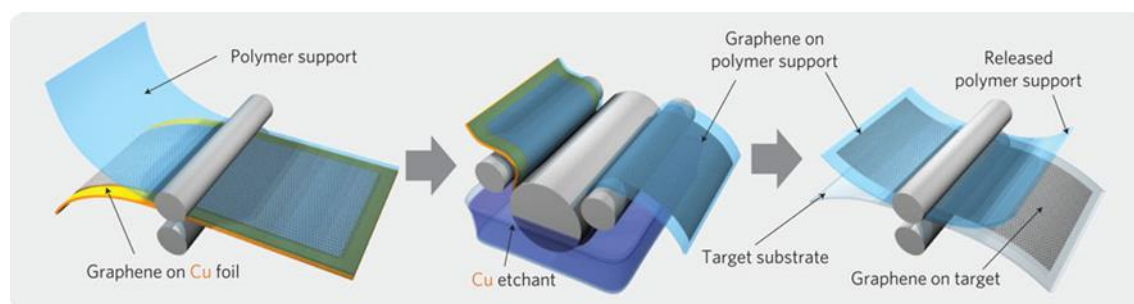


Figure 2.5: Schematic of the roll-based production of graphene films grown on a copper foil.

2.3.4 Mechanical Assisted Liquid Phase Exfoliation of Graphite into Graphene

Graphene can be successfully exfoliated with a scalable production in liquid environment by introducing ultrasound to extract individual layers (Lavin et al., 2016). This method are usually assisted in liquid environment which involves three major steps: [1] dispersion of graphite in solvent, [2] exfoliation, [3] purification (Artur Ciesielskia and Paolo Samorì, 2014). Typically, Graphene flakes can be produced by surfactant-free exfoliation of graphite via chemical wet dispersion. Followed by ultra-sonication in organic solvent before it will be introduce to the centrifugal and freeze dry to obtain graphene powder.

Liquid exfoliation of graphene, also referred to as solution based graphene exfoliation, was first carried out by the Coleman group in 2008 via sonication of graphite flakes in organic solvents such as N-methyl-pyrrolidone (NMP) and dimethylformamide (DMF) (Coleman et al., 2008). Coleman's work stemmed from previous research involving dispersion of CNT in organic solvents which was concerned with matching the surface energies associated with CNT and the solvent. The use of surfactants in liquid exfoliation is also carried out to create aqueous dispersion of graphene help mitigate colloidal aggregation of graphene in solution.

Other less common but noteworthy liquid exfoliation methods include intercalation of graphite with alkaline or halogen salts to form graphite intercalation compounds (GICs). The GIC's can be either directly dispersed and exfoliated in solution by sonication or also thermally expanded at high temperatures in which the intercalating compounds volatilize to form expanded graphite (EG) (Nikitin & Pyatkovskii, 1997) which is subsequently exfoliated in solution via sonication.

Liquid exfoliated graphene is advantageous compared to methods such as epitaxial growth, CVD growth and mechanical exfoliation due to the simplicity of the process which does not require high vacuum and high temperatures as well as the low cost of the starting materials. Solution processing of graphene is also more amenable to scale up on an industrial level and lends itself to facile surface application techniques such as spin Coating, ink printing and other deposition methods to substrates not requiring transfer from a growth substrate (Cummins & Desmulliez, 2012).

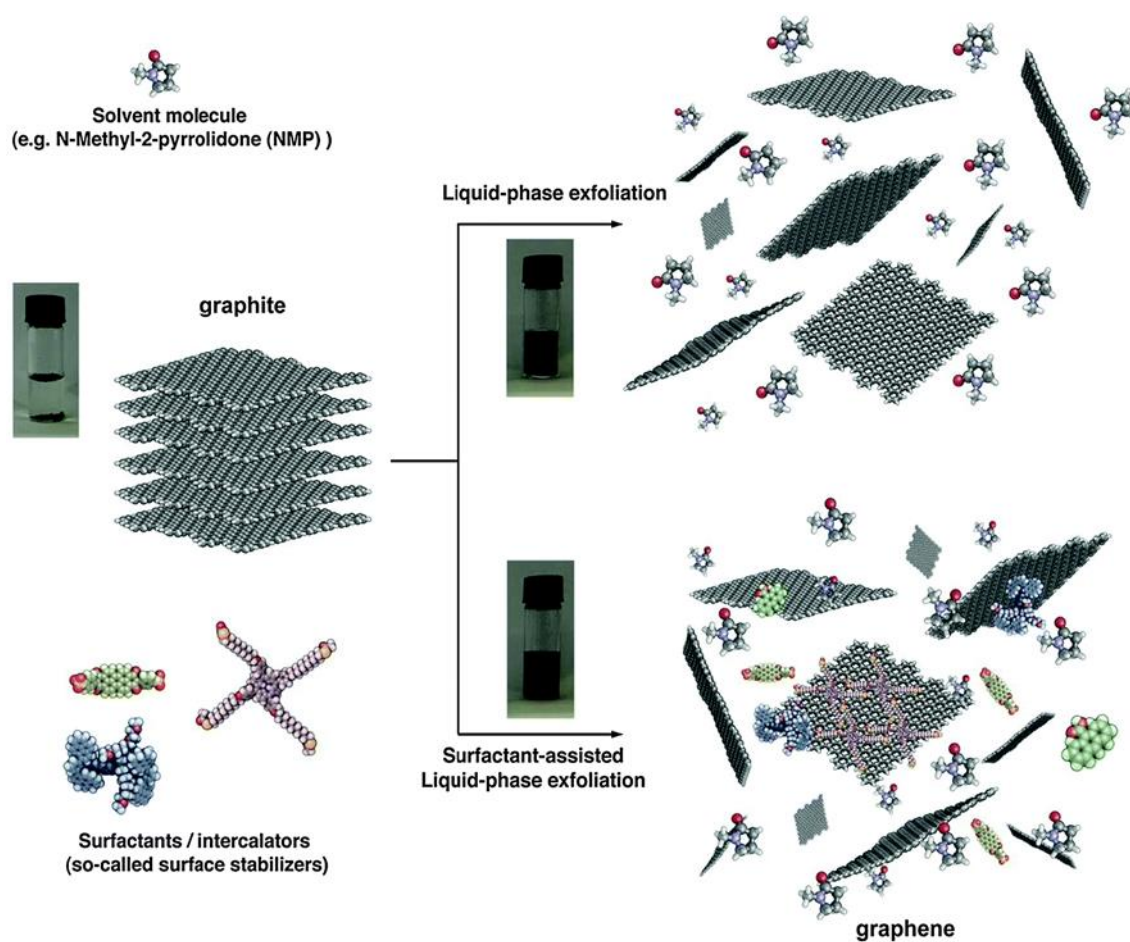


Figure 2.6: Schematic representation of the liquid-phase exfoliation process of graphite in the absence (top-right) and presence (bottom-right) of surfactant.

2.4 Effect of Processing Parameters

2.4.1 Time

Since the first successfully exfoliation of graphene via sonication in organic solvent such NMP in 2008, this dispersion using drastically longer sonication time (~500 h). Such a time consuming approaches requires high energy consumption. In addition, as previously observed for nanotubes, with the increasing sonication time, the size of the flake produce is severely reduced. Which make it more important and critical parameter for several application. Beside than reduced size flake, both long and short sonication time of graphite can affect the quality of graphene. Shortcoming of sonication can intrinsically attributed to the sonication induced cavitation that eventually can cause more defect to the graphene produced (Bracamonte et al., 2014). Though cavitation is favourable for exfoliation, it is relatively harsh process which can produce high local temperature (~ several thousand K), extreme pressure (~ several thousand atm), and rapid heating/cooling rates (~ several billion K/s) (Flint & Suslick, 1991). These harsh conditions that involved in cavitation could result in damage to the graphene. The analysis of Raman spectra can provide information on the number and position of broken-conjugation areas in graphene which is sometimes called point-defect that can effect electronic properties of graphene and it is reported that defect localization strongly depends on a sonication time. This defect are usually located at the edges of graphene flake, whereas the basal plane of flakes is relatively defect free (Henrich et al., 2007).

For CVD, in previous experiment, report shown that in a short growing time, bi- or few-layered graphene with defects such as grain boundary and crack can be synthesized. But with the increasing growing time, D peak will gradually reduce which as shown in Raman spectra result in figure 2.7. Because, by increasing growing time, upper layer might be covered on a defected part of a bottom layer and D peak will be severely reduced. However, the number of layer will increased from 2~3 to over 15 which is effect the quality of graphene produce (Jungrok et al., 2012).

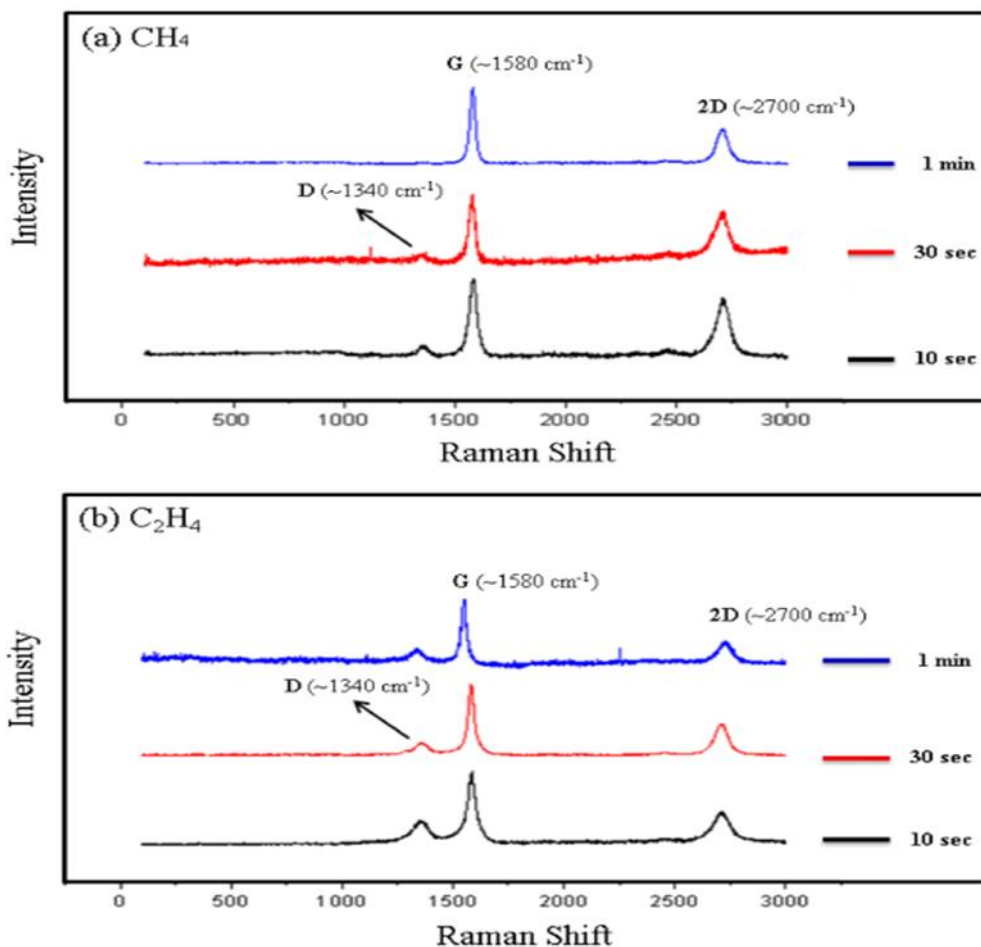


Figure 2.7: Raman spectra of the graphene grown at different growing time with (a) 15:1 ($H_2:CH_4$) and (b) 15:1 ($H_2:C_2H_4$) of gas mixing ratio at 950 °C.

2.4.2 Temperature

In CVD, Jungrok et al reported that the D peak was reduced gradually by increasing growing temperature (Jungrok et al., 2012). This is due to the high temperature caused a stable structured and high quality graphene synthesis. However, CVD growth of graphene by using very high temperature may not be suitable for many substrates or structures. As an alternative, Plasma Enhanced Chemical Vapor Deposition (PECVD) has been explored for the low temperature growth of graphene. PECVD allows lower temperature as the energy required to break the bonds is supplied through plasma (Chugh et al., 2015). In his experiments he used temperatures of 650°C to decompose CH_4 by plasma for a range between 1-15 minutes. The gases were introduced at pressure 1 m Torr and a flow rate of 6 sccm. The system was cooled down at a rate of approx. 150°C / min in a 100sccm flow of argon at a pressure of 1 Torr. He claimed that while copper was used to speed up

the process as a catalyst and it is not necessary condition to grow graphene. He also mentioned that low temperature; rapid, non-catalytic synthesis is needed for industrial mass production of graphene device.

For exfoliation via sonication, it is stated that when the graphene and solvent surface energy is closed, the exfoliation occurs more easily. The good solvent tend to have a surface energy of $70\text{-}80\text{ mJ/m}^2$. However these result are obtained at room temperature and short sonication time. If the temperature is elevated, the surface energy and the surface tension will changed. If the sonication is intensive, the solvent would suffer from degradation and their properties will also be change and eventually make the large-scale production of graphene by sonication fail. Therefore, the solvent surface energy should be tuned with aspect to temperature (Kim et al., 2015).

2.4.3 Sonication power

In term of sonication power, by increasing the sonication power, graphite flakes receive more energy through sonication that result in better stability of graphene dispersion during the process which improves the yield. This is important because in order to use the high concentration suspension of few layers or monolayer graphene for several applications, the graphene suspension must exhibit long term stability. In this regards, an experiment was conducted to study and the stability of graphene suspensions were judged for a month by using following two strategies, which are, (a) low power bath sonicator and (b) high power probe sonication. It is observed that graphene suspension sonicated by high power probe sonication shows that the graphene suspension was stable even after 30 days, while the graphene suspension sonicated using low power bath sonicator showing the sedimentation of the graphene Nano sheets. Thus, the sonication strategy of high power probe sonication is an effective strategy to obtain the long term stability of graphene suspension. The sonication power was varied in the range of 80-160W and the result will show the positive influence of this parameter on the yield (Rakhee et al., 2014).

2.4.4 Centrifuged Speed

The majority component of the material in dispersion after sonication is composed of thick graphite-like flakes, which can be removed by differential ultra-centrifugation (sedimentation-based separation, SBS). Theoretically, beside enriching the graphene produce, SBS is the process where it separates particles on the basis of their sedimentation degree in response to centrifugal force acting on them (Watson, 2011). It is highlighted that LPE generally produce flakes with lateral size of one micrometer or less hence being too small for many application (Gong et al., 2013). To address this issue, an experiment was carried away to describe that by centrifuging at concentration dispersion at 4000 rpm, they manage to separate the smallest flakes into the supernatant from the larger ones in the sediment. The sediment was redispersed and centrifuged at 3000 rpm. This again separated smaller (supernatant) from larger flakes (sediment). This procedure was repeated a number of times until a centrifugation rate of 500 rpm was reached. Then, the flakes size in each supernatant is characterised by using Raman spectroscopy (Khan et al., 2011). The result is the flake size increase from $\sim 1 \mu\text{m}$ for the 4000 rpm sample to $\sim 3 \mu\text{m}$ for the 500 rpm sample (figure 2.8).

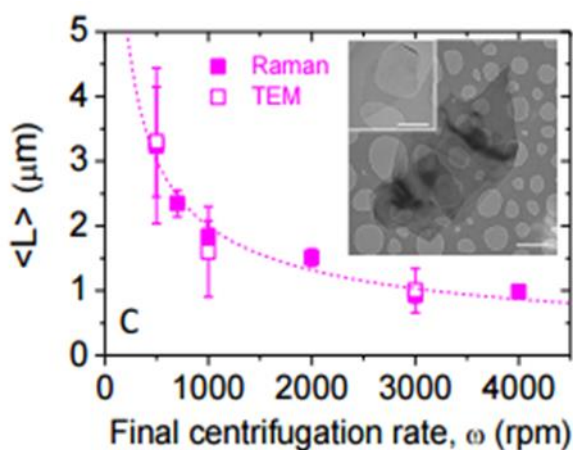


Figure 2.8: Length of size selected flakes plotted as a function of final centrifugation rate. Flakes found after final centrifugation at 3000 rpm (small flake) and 5000 rpm (large flakes).

2.4.5 Solvent

The distance between stacked parallel graphene layers in bulk graphite amounts to 3.35 Å. Although the van der Waals attractions among adjacent layers are weak enough to let them slide on each other in the direction perpendicular to the c-axis, the attraction is strong enough to make complete exfoliation into individual layers challenging. The first attempt by Brodie to produce single-layer graphene sheets by exfoliation dates as far back as 1859 (Brodie, 1859). Since then, many unsuccessful attempts have been made to come up with solutions for the large-scale production of graphene. Successful exfoliation requires the overcoming of the van der Waals attractions between the adjacent layers. One of the most effective and straightforward methods to reduce the strength of the van der Waals attractions is liquid immersion, where the potential energy between adjacent layers is contributed by the dispersive London interactions, which in the presence of a solvent are significantly reduced with respect to vacuum. In the past decades, it has been found that interfacial tension plays a key role when a solid surface is immersed in a liquid medium. If the interfacial tension between solid and liquid is high, there is poor dispersibility of the solid in the liquid (Israelachvili, 2011). In the case of graphitic flakes in solution, if the interfacial tension is high, the flakes tend to adhere to each other and the work of cohesion between them is high (i.e. the energy per unit area required to separate two flat surfaces from contact) hindering their dispersion in the liquid.

Solvents with surface tension (the property of the surface of a liquid that allows it to resist an external force, due to the cohesive nature of its molecules) $\gamma \sim 40 \text{ mJ m}^{-2}$ are the best solvents for the dispersion of graphene and graphitic flakes, since they minimize the interfacial tension between solvent and graphene. Unfortunately, the majority of solvents with $\gamma \sim 40 \text{ mJ m}^{-2}$ such as N-methyl-2-pyrrolidone (NMP 40 mJ m^{-2}), N,N-dimethylformamide (DMF 37.1 mJ m^{-2}), and ortho-dichlorobenzene (o-DCB 37 mJ m^{-2}) have some issues such as relative stability, long sonication periods, expensive solvents and the excessive use of surfactants are limiting factors in the production of the graphene (Lotya et al., 2010). Furthermore this solvent have some disadvantages which is toxicant and particularly having high boiling point, therefore making it hard to separate and remove the solvent after exfoliation (Nicolosi et al., 2013).

Water is a natural choice because of its non-toxicity which opens perspective for the formation of biocompatible graphene based materials for biomedical applications. But, the exfoliation of graphene in water is particularly challenging due to the hydrophobic nature of the sheets. However, such a challenge can be overcome by using surfactants which allow exfoliated sheets to remain suspended (Bourlinos et al., 2009). Therefore, the key challenge in producing graphene sheets was the exfoliation of graphite in a suitable solvent or surfactants that could disperse highly stable graphene sheets in large quantities.

2.4.6 Pressure

In recent years, LPE with aid of pre-intercalation to the exfoliation process can improve the yield of graphene produce by using jet cavitation device (JCD), a high jet pressure (~20 MPa). Passing through the cavitation generator of the JCD system, the graphite-containing solution forms a particle laden cavitating flow, in which the exfoliation of graphene is participated mainly by two kind of stresses.

Firstly, in the high velocity region of the fluid where the local pressure become very low, cavitation bubbles consisting of water vapour and causes the desorbed air will nucleate, grow and then collapse when conveyed to higher pressure regions, inducing micro jets and shock wave with high pressure and velocities. So, exfoliation effect can be achieved by the tensile stresses derived from graphite-solution interfacial reflection of compressive wave.

Secondly, a turbulence jet is caused by the high pressure difference between the inlet and outlet of the cavitation generator and high hydrodynamic stresses are thus created, which may also be contributory to the exfoliation process. It is reported that the particle-laden turbulent flow, the interaction between the particles and the fluid strongly depend on the volume fraction of particles and higher content of particle will exert greater impact on the carrier flow, for example altering the turbulent structure which cause the graphite to be highly exfoliated (Liang et al., 2015).

2.5 Graphene Characterization Tools

2.5.1 Raman Spectroscopy Analysis

Raman spectroscopy is one method currently used to determine how many layers of graphene are present in a present sample. It utilizes the process of Raman scattering to identify what materials are present in a specific sample by analyzing the shift in wavelength of light that is scattered off of a material, which is different for different materials.

There are two primary types of scattering that occur when light strikes a material: Rayleigh and Raman scattering. In Rayleigh scattering, a photon of a given energy and wavelength interacts with a molecule in a material and raises it to a virtual energy state. After a moment, the molecule comes back down to its original energy state, releasing another photon. Since the molecule came back down to its original energy state after being raised, the released photon has the same energy (and thus wavelength) as the incident photon; thus, Rayleigh scattering can be referred to as an elastic process (the energy of the photon being conserved).

In Raman scattering, a photon of a given energy and wavelength also interacts with a molecule in a material and raises it to a virtual energy state, as in Rayleigh scattering. However, when the molecule drops from its virtual energy state, it may drop not to its original state but to a state above or below its original energy state. When the molecule drops to a lower state it releases a photon; however, the energy of the photon is not the same as that of the incident photon. The energy of the released photon is dependent on the final energy state of the molecule. If the final energy state of the molecule is greater than its original ground state, then the released photon will have a lower energy than the incident photon, and thus a longer wavelength; this is referred to as Stoke's Raman scattering. However, if the final energy state of the molecule is lower than the original initial state, then the released photon will have a higher energy than the incident photon, and thus a shorter wavelength – anti-Stokes Raman scattering. Since the energy of the photons is not conserved, Raman scattering is a form of inelastic scattering. Figure 2.9 for a visual representation of all three types of scattering and the differences between their elastic and inelastic properties.

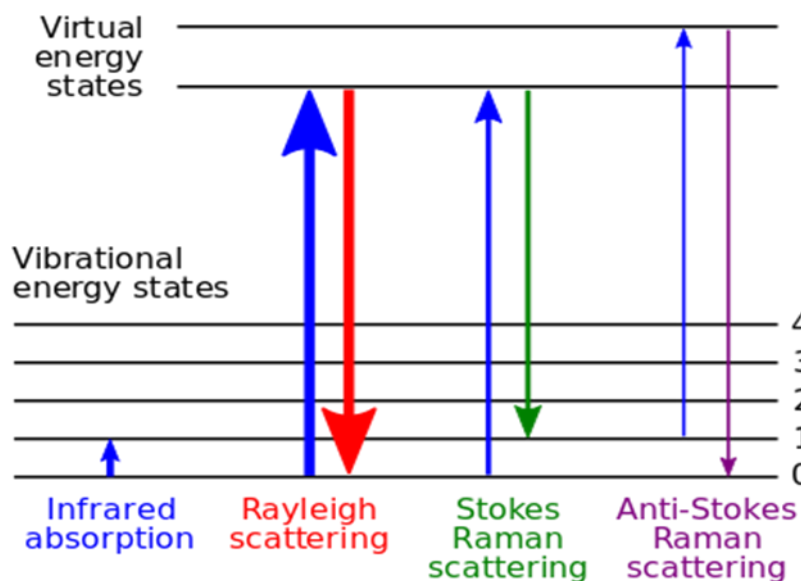


Figure 2.9: Energy level diagram show the states involved in Raman signal

In all types of Raman scattering, the energy removed from or transferred to the photon is related to specific phonons – i.e. lattice vibrations- of the target material. Thus, only certain changes in photon energy, and thus wavelength and frequency, are possible. These frequency shifts are different for every material, which means that measurements of the shift in frequencies in the scattered photons can shed light on the identity of the material in question. The shift depends on the energy of the spacing of the molecule's modes. However, not all modes appear in the Raman spectra, only those that do involve changes in the polarizability, α , of the molecule being analyzed. The polarizability depends upon the bond lengths in the molecule, with shorter bonds being more difficult to polarize. In crystalline solids, the modes are determined by the crystal structure, which can be determined from the polarization of the scattered light. If the polarizability of a molecule is changing, then the molecule is vibrating, which induces a dipole moment. Oscillating dipole moments release photons, and that in conjunction with changing polarizabilities produces Stokes and anti-Stokes scattering.

Raman spectroscopy has significant advantages over other types of spectroscopy (such as infrared) for many reasons: it's non-destructive, does not require any sample preparation, does not require a vacuum, can produce results quickly and produce spatially resolved maps of the different forms of carbon within a specimen (Praver and Nemanich, 2004), and can be used on solids, liquids, gases, and aqueous solutions (infrared

spectroscopy readings are complicated by readings of the water solute). It can also be used in a wide range of temperatures and pressures and on small sample areas. Fiber optic cables can also be used to transmit readings, which is useful for remote testing. However, Raman spectroscopy cannot be used to analyze metals or alloys because the incident beam mainly reflects without scattering. It can also be difficult to measure small concentrations of materials in a mixture because of the low rate of Stokes scattering. Usually, only Stokes lines are used for Raman spectroscopy because anti-Stokes becomes weak if the frequency of vibrations increases. Moreover, the selection rules for the Raman scattering are determined by the theory of photons scattering and the group theory (Malard et al., 2009).

2.5.2 AFM Analysis

Atomic force microscopy (AFM) is used in characterizing a variety of specimens such as biological, semi-conductor, and polymer samples. AFM can provide information regarding surface morphology in micro-and nano scale. A common AFM system figure 2.10 includes a piezoelectric (PZT) actuator, a sharp tip which is placed in the top of the cantilever probe, a sensitive photo detector, and a monochromatic light. The principle of AFM employs a tip that scans the surface of the sample at a constant height and force that is provided by PZT. The end-point of the laser beam impinges the cantilever, then deflects the light to the sensitive photo detector. The different light intensities and phases measured by photo detractor provide information about the surface (Jalili & Laxminarayana, 2004)

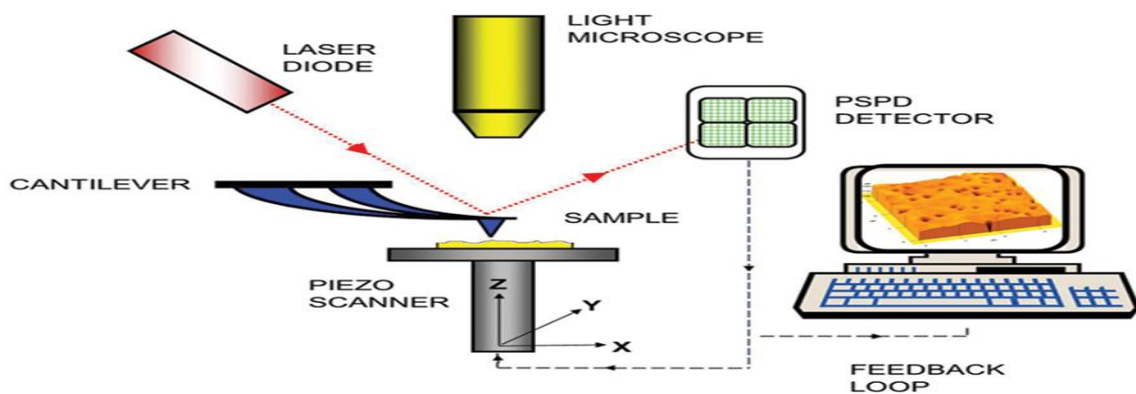


Figure 2.10: A schematic representation of the AFM

The AFM has three open-loop modes: contact mode, non-contact mode, and tapping mode. In contact mode the tip is in mechanical contact with the sample, whereas in non-contact mode the cantilever oscillates near the surface of the sample. In tapping mode the contact and non-contact methods are employed so that the cantilever tip touches the sample and oscillates in resonance frequency

2.5.3 XRD Analysis

About 95% of all solids can be described as crystalline. When X-rays interact with a crystalline substance (phase), one gets a diffraction pattern. Every crystalline substance gives a specific pattern; the same pattern; and in a mixture of substances each produces its pattern independently of each other. The x-ray diffraction pattern of a pure substance is therefore, like a fingerprint of the substance. The powder diffraction method is thus ideally suited for characterization and identification of polycrystalline phases.

Crystalline materials are characterized by the orderly periodic arrangements of atoms. If broken down to smaller pieces the structure of a crystal can be found to consist of an identical self-repeating structure called a unit cell. Inside the unit cell many planes exist, these are used to define directions and distances in the unit cell.

XRD (x-ray diffraction) instrument essentially consists of a monochromatic x-ray emitter, a sample holder and a detector figure 2.11. As the beam sent from the emitter hits the sample the wave fields interfere with each other constructively or destroy each other depending on the alignment of the crystallographic planes in the sample. By changing the angle $\psi/2\theta$, peaks in the received reflection from the sample will appear. These depend on the fact that randomly oriented crystals in a sufficient number produce a continuous Debye cone. In a linear diffraction the detector scans through an arc that intersects each Debye cone at a single point thus giving the appearance of a discrete diffraction peak.

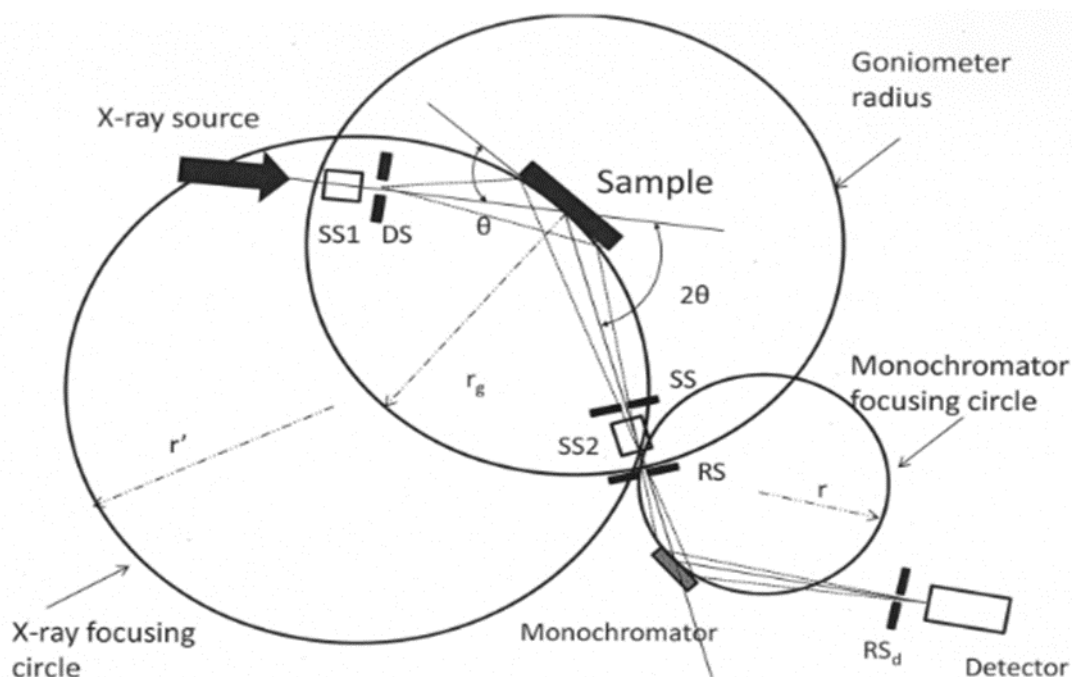


Figure 2.11: Schematic principle of operation of the XRD

2.5.4 UV-VIS Analysis

Spectrophotometers are mainly used to measure transmission or absorption in liquids and transparent or opaque solids. It does so by sending a beam of light through the sample and then monitoring the remaining light in a detector. In the case of a UV-Vis spectrophotometer the light is in the wavelength of 800-200nm, probing electronic transitions in the sample. It is hard to reach a lower wavelength than 200nm as oxygen starts to absorb light below that wavelength. When the light passes through the sample some of the molecules in the sample will absorb lights at various wavelengths of this spectrum, depending on their chemical bonds and structure. As a rule energetically favored electron promotion will be from the highest occupied molecular orbital (HOMO) to the lowest unoccupied molecular (LUMO), and the resulting species is called an excited state. When sample molecules are exposed to light having an energy that matches a possible electronic transition within the molecule, some of the light energy will be absorbed as the electron is promoted to a higher energy orbital. A spectrophotometer records the wavelengths at which absorption occurs, together with the degree of absorption at each wavelength. The resulting spectrum is presented as a graph of absorbance versus wavelength.

2.5.5 FESEM Analysis

Field emission scanning electron microscopy (FESEM) provides topographical and elemental information at magnifications of 10x to 300,000x, with virtually unlimited depth of field. Compared with conventional scanning electron microscopy (SEM), FESEM produces clearer, less electrostatically distorted images with spatial resolution down to 1/2 nanometers – three to six times better.

FESEM operate with electrons are liberated first from a field emission source and accelerated in a high electrical field gradient. Within the high vacuum column these so-called primary electrons are focused and deflected by electronic lenses to produce a narrow scan beam that bombards the object. As a result secondary electrons are emitted from each spot on the object. The angle and velocity of these secondary electrons relates to the surface structure of the object. A detector catches the secondary electrons and produces an electronic signal. This signal is amplified and transformed to a video scan-image that can be seen on a monitor or to a digital image that can be saved and processed further. Therefore it suitable analysis in order to study for the morphology and structure of graphene.

2.5.6 TEM Analysis.

The transmission electron microscope (TEM) is a very powerful tool for material science. A high energy beam of electrons is shone through a very thin sample, and the interactions between the electrons and the atoms can be used to observe features such as the crystal structure and features in the structure like dislocations and grain boundaries. Chemical analysis can also be performed. TEM can be used to study the growth of layers, their composition and defects in semiconductors. High resolution can be used to analyze the quality, shape, size and density of quantum wells, wires and dots (Williams and Carter ,2009)

The TEM operates on the same basic principles as the light microscope but uses electrons instead of light. Because the wavelength of electrons is much smaller than that of light, the optimal resolution attainable for TEM images is many orders of magnitude

better than that from a light microscope. Thus, TEMs can reveal the finest details of internal structure - in some cases as small as individual atoms.

The beam of electrons from the electron gun is focused into a small, thin, coherent beam by the use of the condenser lens. This beam is restricted by the condenser aperture, which excludes high angle electrons. The beam then strikes the specimen and parts of it are transmitted depending upon the thickness and electron transparency of the specimen. This transmitted portion is focused by the objective lens into an image on phosphor screen or charge coupled device (CCD) camera. Optional objective apertures can be used to enhance the contrast by blocking out high-angle diffracted electrons. The image then passed down the column through the intermediate and projector lenses, is enlarged all the way.

The image strikes the phosphor screen and light is generated, allowing the user to see the image. The darker areas of the image represent those areas of the sample that fewer electrons are transmitted through while the lighter areas of the image represent those areas of the sample that more electrons were transmitted through.

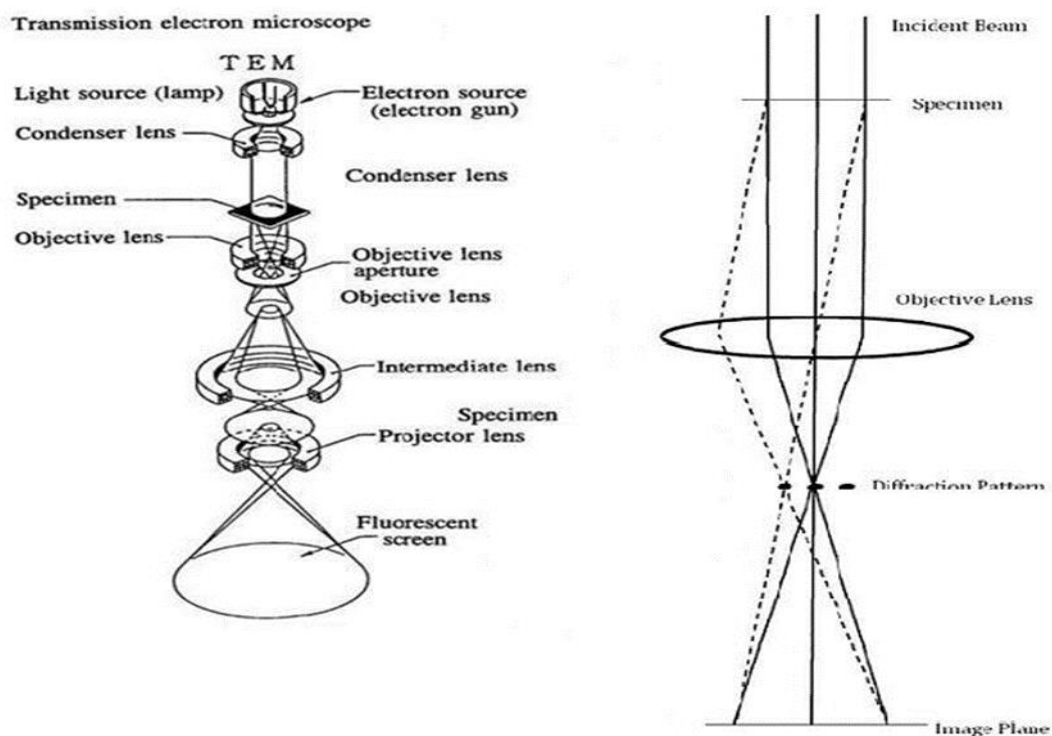


Figure 2.12: General layout of a TEM describing the path of electron beam in a TEM and a ray diagram for the diffraction mechanism in TEM.

2.5.7 FTIR Analysis

Fourier Transform-Infrared Spectroscopy (FTIR) is an analytical technique used to identify organic (and in some cases inorganic) materials. This technique measures the absorption of infrared radiation by the sample material versus wavelength. The infrared absorption bands identify molecular components and structures. When a material is irradiated with infrared radiation, absorbed IR radiation usually excites molecules into a higher vibrational state. The wavelength of light absorbed by a particular molecule is a function of the energy difference between the at-rest and excited vibrational states. The wavelengths that are absorbed by the sample are characteristic of its molecular structure.

The FTIR spectrometer uses an interferometer to modulate the wavelength from a broadband infrared source. A detector measures the intensity of transmitted or reflected light as a function of its wavelength. The signal obtained from the detector is an interferogram, which must be analyzed with a computer using Fourier transforms to obtain a single-beam infrared spectrum. The FTIR spectra are usually presented as plots of intensity versus wavenumber (in cm^{-1}). Wavenumber is the reciprocal of the wavelength. The intensity can be plotted as the percentage of light transmittance or absorbance at each wavenumber

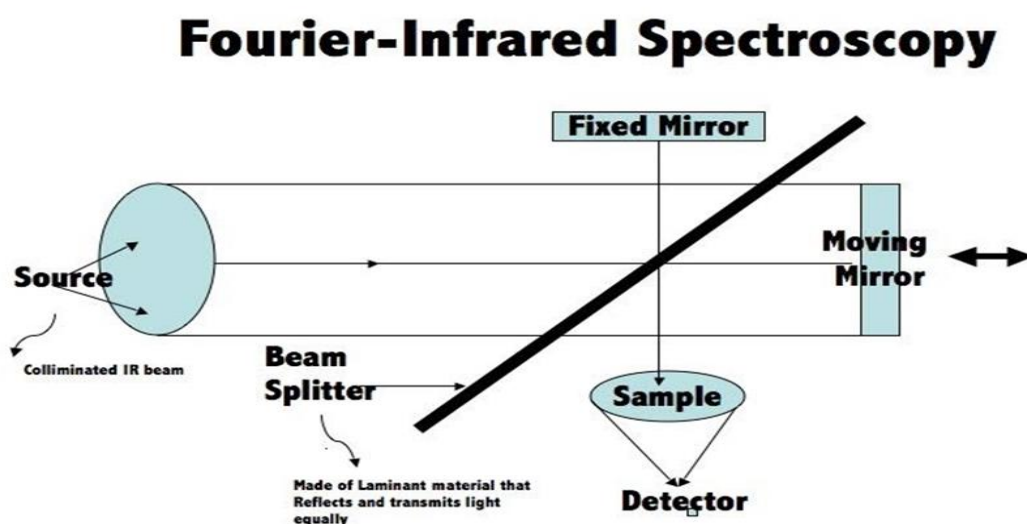


Figure 2.13: Illustrates how the FTIR instrument works.

2.5.8 Structure of Thesis

In this research, the green and environmental approach is approach to exfoliate graphene via sonication using water and tea leaf. Water is chosen because of its non-toxicant and abundancy. The sonication will be direct sonication using homogenizer in order to archive high yield and complete exfoliation. To study the effect of parameter, the sonication will be conducted at different power (40% and 50%), different centrifugation speed (5000rpm and 8000rpm), and different sonication time (1h, 2h, 3h and 5h).

CHAPTER 3

METHODOLOGY

3.1 Materials

In this research, the most important material for sample processing is graphite. Graphite was bought from Sigma Aldrich, America. It was used in the liquid phase exfoliation of graphite by using ultrasonication to promote the intercalation and expansion of graphite with selected solvent.

Table 3.1: Graphite properties

Physical state	Solid
Molecular weight (<i>g/mol</i>)	12
Relative Density (<i>g/cm³</i>)	2.09-2.25
pH	None
Colour	Black/ Grey
Odour	Odourless

3.2 Graphene preparation

For graphene preparation, graphite flakes (0.5g) will be dispersed in the mixture of 300ml of ultrapure water and tea leaf (filtered). To exfoliate the 2D material we will use a homogenizer. The operation power for the homogenizer will be set at 40% and 50% for 2 hours. In addition the solution will be sonicated at atmospheric condition (20°C). The resulting solution will then be centrifuged at 5000 rpm and 8000 rpm for 1 hour. Then the suspension will be removed using pipette and filtered using vacuum filter. To study the relation between homogenizer power and centrifuge speed in exfoliation of graphite, graphene dispersion will then first be analysed using UV-Vis spectroscopy. The parameters which give the highest value of absorbance are then repeated but using different sonication time. Lastly, the graphene product will be introduced into a freeze dryer to remove water.

content before being characterize using various method analysis. For a comparison, the sonication time will be set at 1hour, 3hour and 5 hour.

Table 3.2: Summary of experiment sample

Sample	Power	Speed (rpm)	Time (hour)
GZ1	40%	5000	2
GZ2	50%	5000	2
GZ3	40%	8000	2
GZ4	50%	8000	2

Sample	Power	Speed (rpm)	Time (hour)
GZ5	40% / 50%	5000/8000	1
GZ6	40% / 50%	5000/8000	3
GZ7	40% / 50%	5000/8000	5

3.3 Characterization techniques

3.3.1 XRD

The basic analysis to know the crystal configuration and orientation of the nano crystalline material. The diffraction pattern results, when the X-rays come in contact with a crystalline phase and show the different orientation and the inter layer spacing of atomic layer.

XRD (Philips D5000 X-Ray Diffractometer) experiments was conducted to analyze the structure of the exfoliated flakes over the diffraction angle range of 2θ (3° – 80°) with Cu K α radiation (wavelength = 0.15406 nm) operated at 40 kV and 300 mA.

3.3.2 UV-Vis

UV-Vis (Hitachi U-1800 spectrophotometer) was used to measure absorption. A beam of light was passed through the sample and remaining of light is monitored in a detector. The light which is being passed through the sample will be absorbed by some of the molecule present on the sample depending upon on their structure and chemical bonding (Vandana et al., 2015). The sample was carried on out with a spectrophotometer over a spectral range of 200–800 nm.

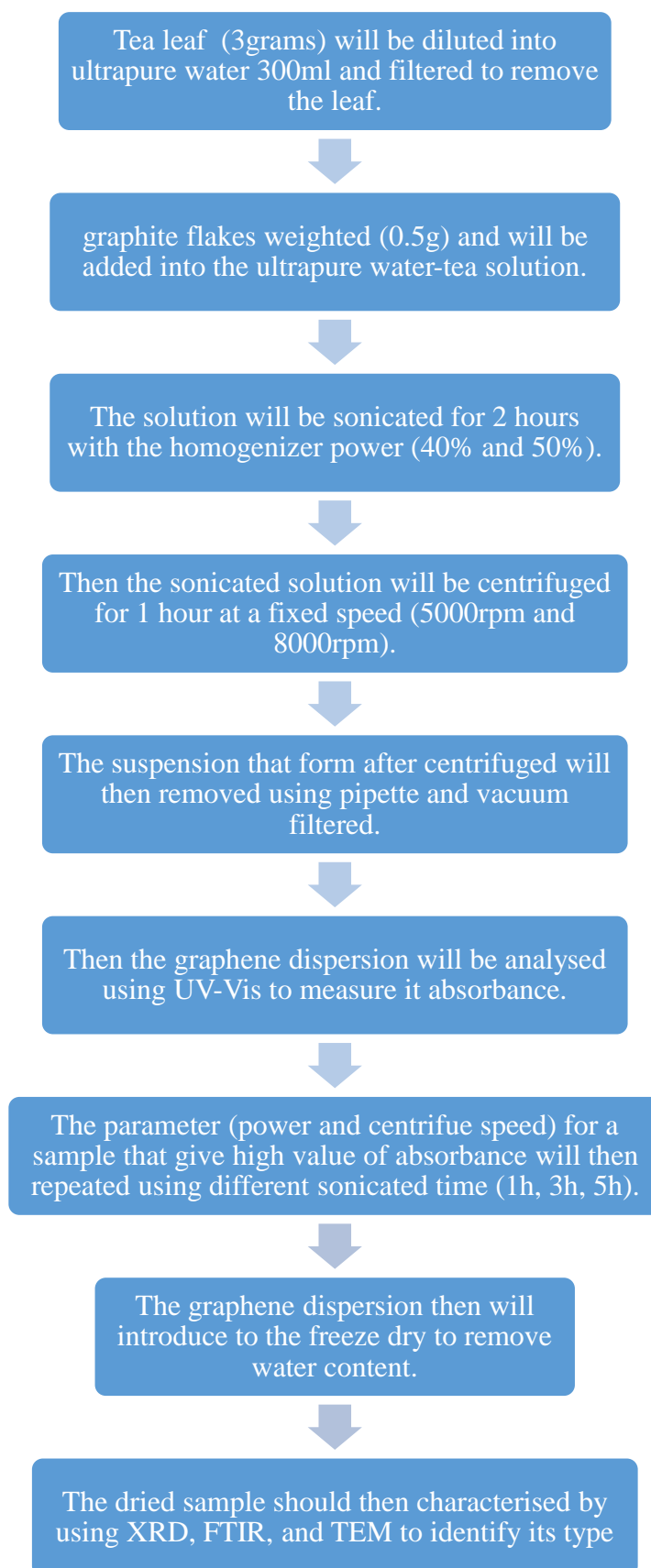
3.3.3 FTIR

FTIR (Nicolet Is-5 FT-IR spectrometer) was used for identification and characterization of functional groups of exfoliated graphite by using range of 400-4000 cm^{-1}

3.3.4 TEM

To study the surface morphology and structural properties of the samples, TEM analysis (Tecnai G2 20 Twin) was operated at 100 kV which allowed the image of graphene sheets and nanoparticles to be gathered.

3.4 Process flow diagram



CHAPTER 4

RESULTS AND DISCUSSION

4.1 Ultraviolet-Visible Spectroscopy (UV-vis) analysis

4.1.1 Concentration of Graphene dispersion

Graphene concentration (C_g) can be determined through absorption from UV-Vis analysis with 1 cm cuvettes, and calculated by Beer-Lambert law (Hernandez et al., 2008). Graphene dispersion spectrum in the range from 200 nm to 800 nm shows that 660 nm is a decent wavelength for characterization. According to Lambert-Beer Law, Absorption of the dispersion equals to a factor ε_{660} multiplies concentration of graphene. As ε_{660} was valued differently by different groups a uniform value of ε_{660} must be determined (Wang et al., 2016). First prepare graphene dispersion through liquid-phase exfoliation, and measure the absorption of the dispersion using UV-Vis with the wave length of 660 nm. The C_g can be determined by the formula:

$$C_g = (m_1 - m_2)/V$$

Where

$m_1 =$ membrane weight after the filtrate (mg)

$m_2 =$ membrane weight before the filtrate (mg)

$V =$ volume of dispersion (ml)

Figure. 4.1 shows A/l as a function of C_g , and ε_{660} can be confirmed by the slope of the fitting straight line and has a relative value of $\left(1002 \frac{ml}{mg.m}\right)$. This result should be attributed to the fact that the surfactant (tea solution) cannot be totally washed off during the filtration process. (m_1-m_2) is the sum of the mass of surfactant and graphene, so the value of C is larger, and the value of ε_{660} is smaller than the actual value.

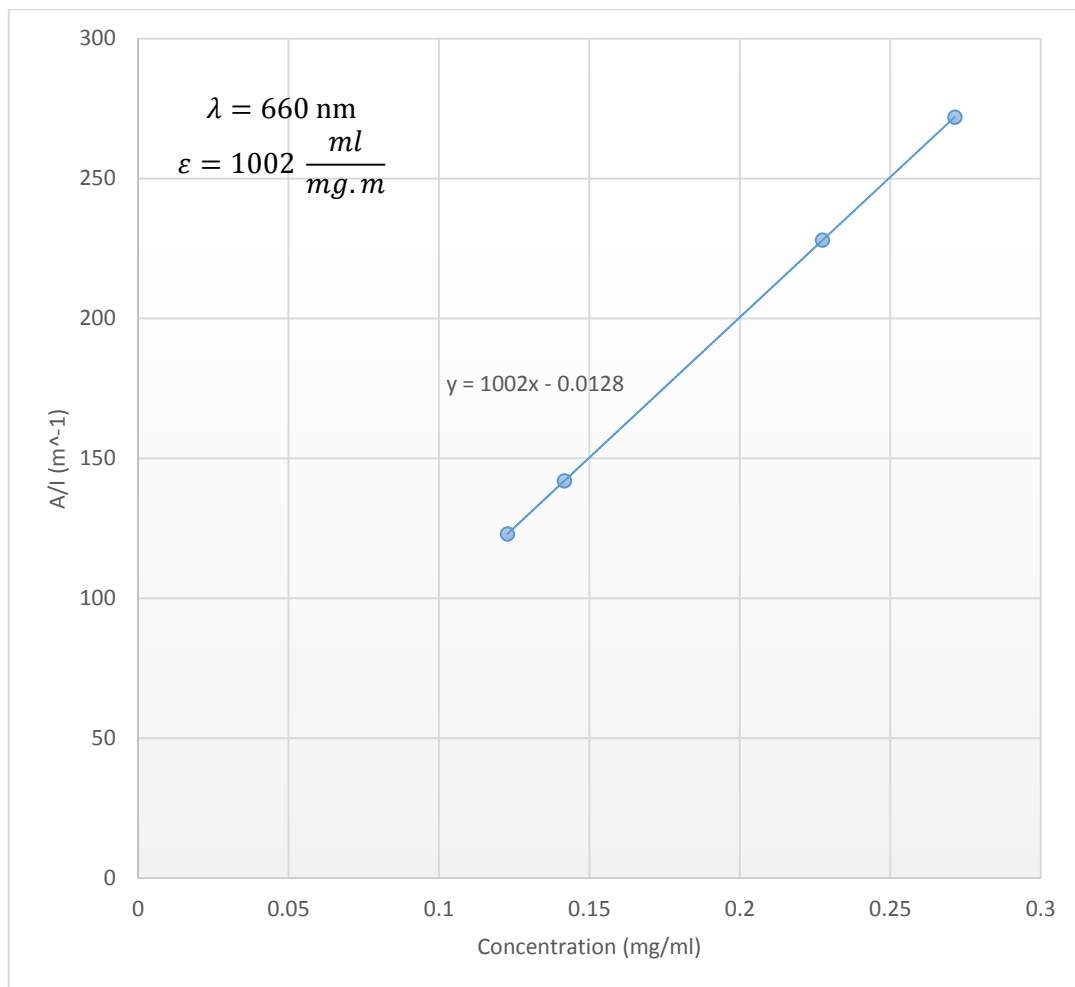


Figure 4.1: Absorption per unit length as a function of C_g .

Three vital factors, sonication time, centrifuge speed and sonication power mainly influence C_g . In order to get a full view of C_g 's dependence on sonication time, other factors must be pre-discussed first.

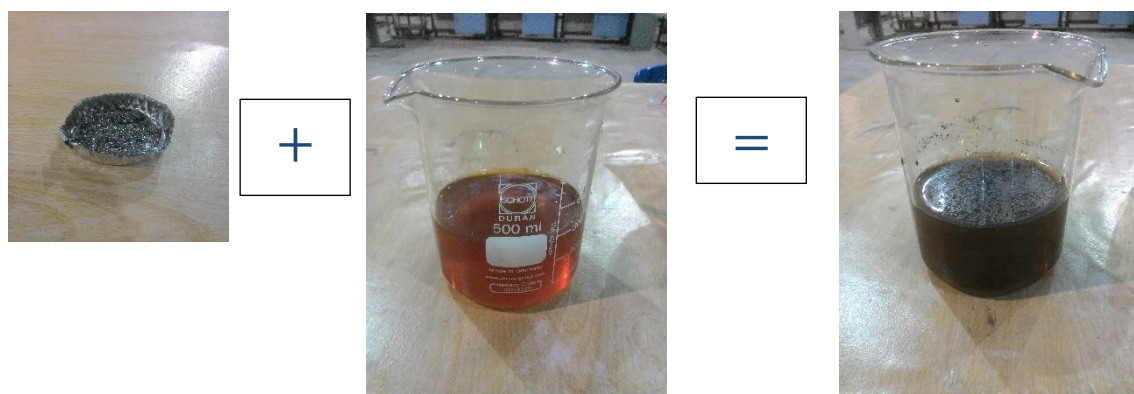


Figure 4.2: Graphite flake added to the ultrapure water-tea solution

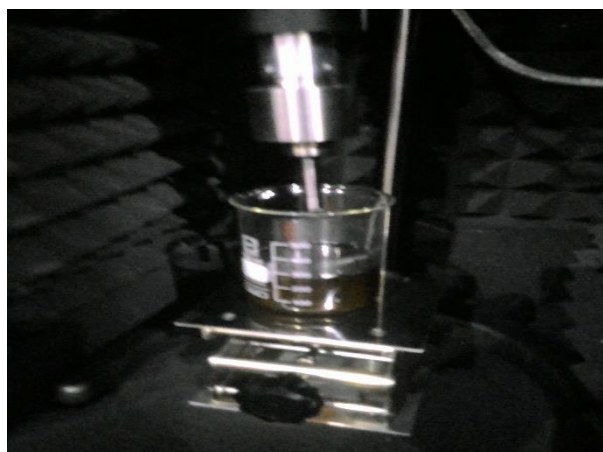


Figure 4.3: Picture of homogenizer used.



Figure 4.4: Picture of graphene dispersion

4.1.2 Concentration as function of sonication power and centrifuge speed

To study the effect of sonication time on graphene concentration, the suitable parameter for sonication power and centrifuge speed need to be considered first. By using OFAT (one-factor-at-a-time) method, the suitable parameters can determined by choosing the sample that gives highest concentration value.

Table 4.4.1: Graphene concentration over sonication power and centrifuge speed

Sample	Power (%)	Centrifuge speed (rpm)	Concentration (mg/ml)
GZ1	40	5000	0.1417
GZ2	50	5000	0.2275
GZ3	40	8000	0.1228
GZ4	50	8000	0.2715

Table 4.1 shows the highest graphene concentration, $0.2715 \text{ mg ml}^{-1}$, was obtained using 50% sonication power and 8000 rpm on centrifuge speed. All the sample were sonicated at 2h period of time. The exfoliation of the nanoparticle in the solvent is occurred due to the strong interaction between the solvent and nanoparticles, means that the energetic penalty for exfoliation and subsequent salvation become small (Zhou et al., 2008). It shown that sample with high sonication power exfoliate higher graphene concentration. Theoretically the absorption values of graphene dispersion sonicated using 50% power probe sonication should be much higher as compared with the graphene dispersion sonicated using 40% power probe sonication. Thus, it is clear from this observation that higher the sonication energy results in higher concentration exfoliation of graphene. This is because, during sonication of graphite flakes in the solvent, the lager flakes is exfoliated into smaller flakes, and subsequently with more amount of energy supplied result in few layers or monolayer with high concentration.

During the sonication process high pressures and high temperatures generated by the implosion of cavitation bubbles cause violent collisions between particles at very high speed. These extreme conditions in sonicated solutions allow solvent dissociation into peroxy radicals (Misik V and Riesz P., 1996). The radical reactions are usually destructive because ultrasonic treatments are very effective in breaking C–C bonds (Guittonneau et al., 2010). Therefore, increasing sonication power result in higher concentration graphene exfoliation.

To test this hypothesis, a researcher group conduct an experiment by comparing graphene concentration exhibit by using high-intensity ultrasound and low-intensity ultrasound waves, such as those generated by the ultrasound bath. They find that high-intensity ultrasound is far more effective than low-intensity ultrasound waves because the exfoliation of graphene concentration is higher by using high power probe sonication as compared to low power probe sonication. Empirically the concentration and energy supplied exhibit linear relationship. The concentration of ~0.12 mg/ml of graphene was achieved by sonicating using bath sonication for 120 minutes, while, sonication using high power probe sonicator yield grapheme of ~1.2 mg/ml for 120 minute (Rakhee et al., 2014). This shows that probe sonication yield is 10 time higher than that of yield obtained using bath sonicator.

To study the effect of the centrifugation speed the sample was prepared and sonicated for 2 hour at 40% and 50% sonication power. The sample was then centrifuged at speeds 5000 and 8000 rpm for 60 min. After centrifugation, two third of the resulting suspension was removed using a pipette and filtered using vacuum filter.

From table 4.1, it shown that there is no significant different and consistent pattern in term of graphene dispersion concentration when vary the centrifuge speed. This is because centrifugation is mainly effect on the quality of graphene, thus, it usually use as a purification. Generally the production of graphene dispersions by LPE inevitably causes a host of polydispersity and other material issues. It is well-known that the material properties of graphene significantly depend on the layer number. Therefore, once the graphite flakes are exfoliated, the next important step is the purification or separation of the exfoliated flakes from the un-exfoliated junk. Centrifugal processing is the most common technique used to separate monodisperse graphene suspensions, where sedimentation rate depends on the shape, size and buoyant density. When a polydisperse graphene suspension is subjected to high centrifugal force, graphene flakes with larger lateral areas sediment faster. As a result, when the centrifugation is completed, smallest flakes are found near the top of the centrifuge tube, whereas the larger flakes are located at the bottom (Rekha and Kim, 2015).

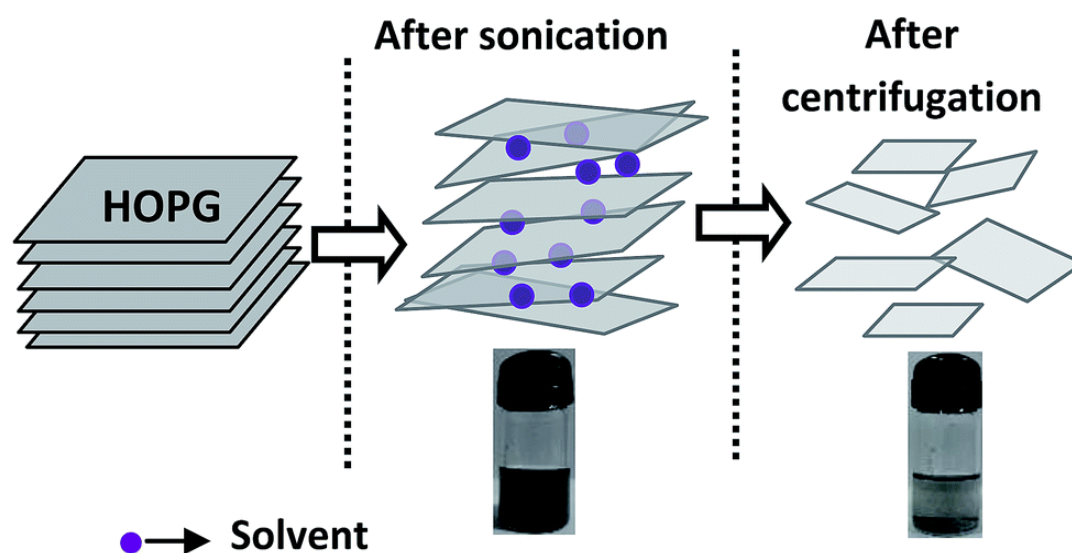


Figure 4.5: Schematic diagram of chemical exfoliation method which illustrate the effect of centrifuge.

It is reported that for centrifuged graphene dispersions, the average lateral flake size decreases as the centrifugation rate increases (Khan et al., 2010). This means that centrifugation at high rate results in the separation of small flakes which remain dispersed from large flakes which sediment out. Many research paper suggest that the sediment can be redispersed resulting in the flakes being separated by size into two different dispersions. They also highlighted that dispersions of sonicated graphite always contain some unexfoliated graphitic crystallites (Hernandez et al., 2008). These must be removed by a centrifugation step with 500 rpm usually enough to remove the graphitic crystallites while leaving the flakes dispersed. Thus, when redispersing the sediment it is always necessary to centrifuge.

According to Umar et al. they find that controlled centrifugation can potentially act as a size selection mechanism (Umar et al., 2012). If one chooses 500 rpm to remove only the crystallites, the result will be the initial supernatant with only small flake, the redispersed centrifuged sediment with all other flake sizes and a second sediment containing the crystallites. However, one could choose a higher centrifugation rate for the redispersed sediment. This would remove crystallites and the largest flakes leaving only medium size flakes dispersed. In this case, the result will be the initial supernatant with only small flakes, the redispersed, centrifuged sediment with medium size flakes and a second sediment with large flakes and crystallites.

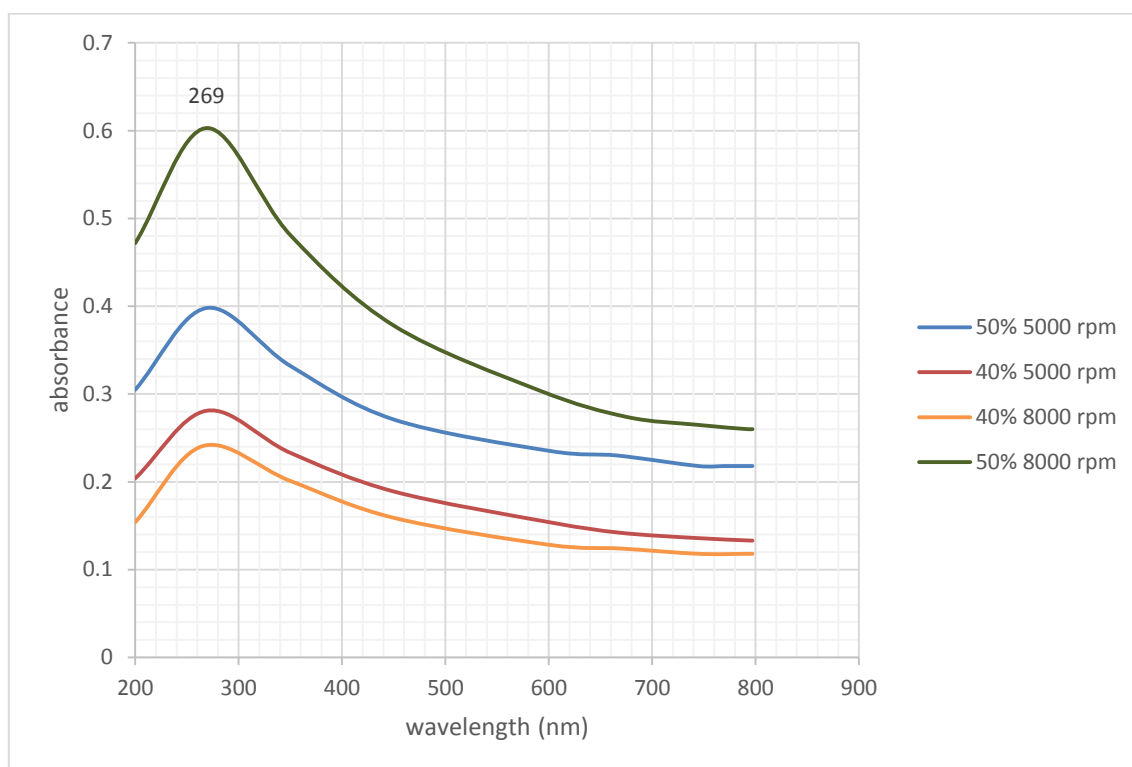


Figure 4.6: UV-Vis spectra of graphene suspensions at different sonication power (%) and centrifuge speed (rpm)

In most of the Uv-Vis spectra analysis of graphene exfoliation, the peak at 273 nm can be used as a confirmation existence of graphene (in our case 269nm) and can be attributed to the $\pi \rightarrow \pi^*$ transitions of aromatic C=C bonds (Liu et al., 2012). However, many research journal highlighted that liquid phase exfoliation usually exhibit 2 peak, indicate mixture of graphene oxide (223 nm peak) and graphene (273 nm peak) (Uran et al., 2017). However, after sonication, no significant peak was observed at 223 nm (characteristic of graphene oxide), in the dispersion solutions, suggesting that ultrasonic treatment prevent significant generation of graphene oxide (Kashyap et al., 2014). Figure 4.6 shown that as the probe sonication power increases, the absorption value at 269 nm also increases, which depict the high concentration exfoliation of graphene. But when we increase the centrifuge rpm, the absorbance value at 269 nm does not show consistent pattern, this is because as mention before, centrifuge speed is mainly effect on the quality of graphene produce.

For all four sample, it was proved that 50% of sonication power and centrifuge speed of 8000 rpm yielded the highest absorption for 200 to 800 nm wavelengths. Other parameter like sonication power (40%) and centrifuge speed (5000 rpm) were eliminated. Therefor to study the effect of sonication time on exfoliation of graphite, parameters like sonication power and centrifuge speed was maintained at fixed value which is 50% and 8000 rpm respectively.

4.1.3 Concentration as function of sonication time

Table 4.4.2: Graphene concentration over sonication time

Sample	Sonication time (hour)	Concentration (mg/ml)
GZ5	1	0.2335
GZ6	3	0.4032
GZ7	5	1.0699

From table 4.2 it is clearly shown sonication for a short period of time only yields low concentration of graphene dispersion. With prolonged sonication, high concentration of graphene dispersion in the ultra-pure water tea solution can be obtained up to 1.0699 mg/ml (5 hour sonication). Although the graphene dispersion have been diluted, it still remain in darker colour which indicates high concentration. This is because as the sonication time increases, more energy can be supplied during the sonication process, thus, increasing the graphene dispersion concentration.

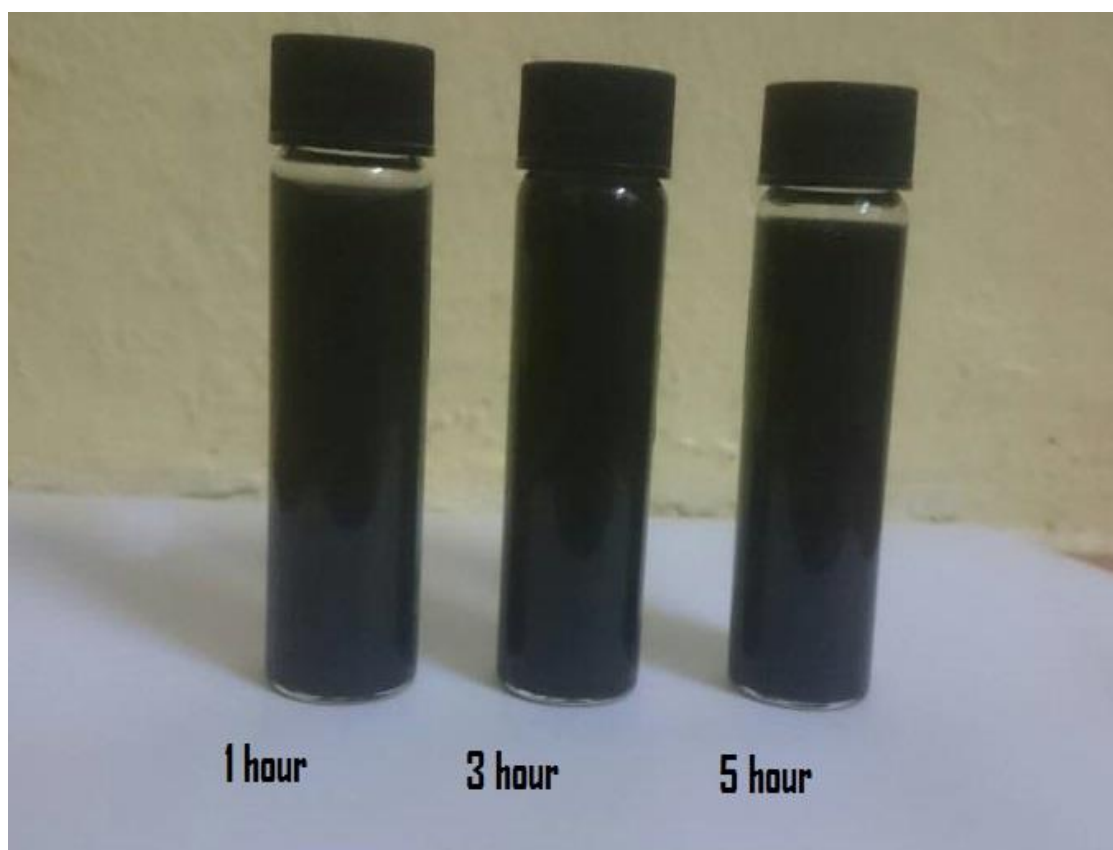


Figure 4.7: Graphene dispersion at different sonication time in ultra-pure water-tea solution. From left: 1hour, 3 hour, 5 hour sonication time.

From figure 4.7, it shows that the colour of the graphene dispersion does not show any different when increase the sonication time. All the 3 sample exhibit darker colour which indicates high concentration of graphene although the sonication time for each sample is different with one another. This may be due to the fact that all the 3 sample is sonicated using homogenizer (direct sonicated at high power). Since van-der Waals bond require low energy to break in order to achieve a complete exfoliation, therefore 1 hour of sonication using high power probe is sufficient to yield high concentration graphene dispersion.

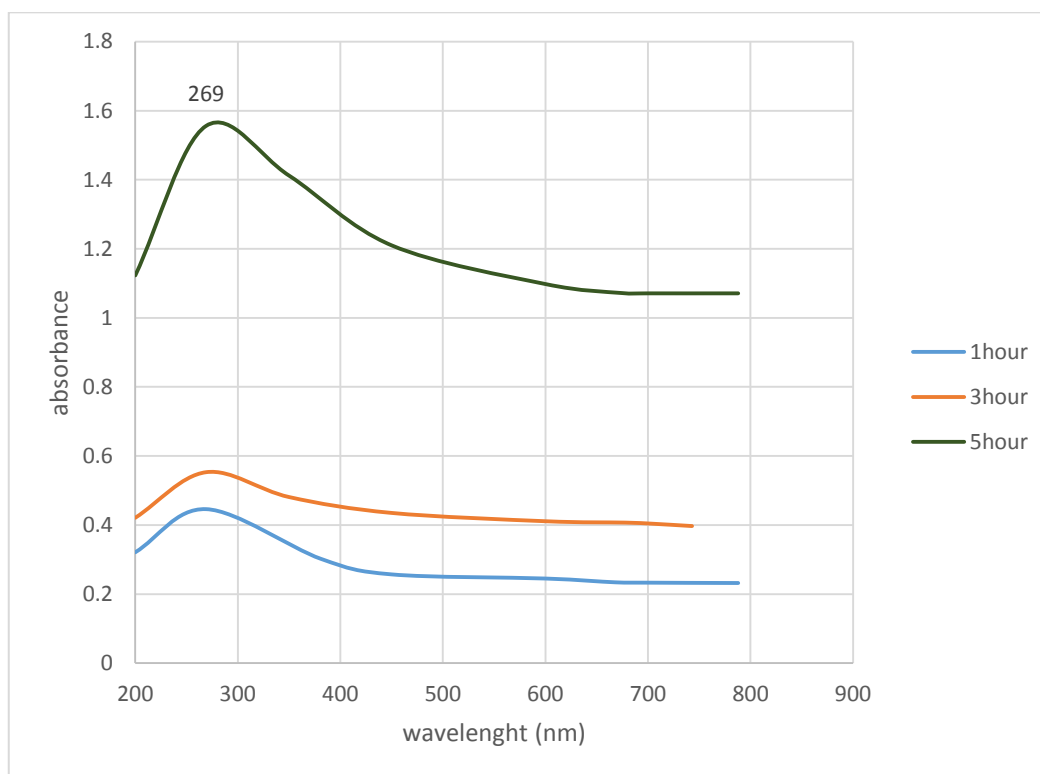


Figure 4.8: UV-Vis spectra of graphene suspensions at different sonication time

UV-Vis spectra in figure 4.8 show almost the same as in figure 4.6 and all the 3 sample exhibit peak value at 269 nm indicating the presence of graphene. As the sonication time increase, the amount of absorbed light will increased thus, absorption at 269 nm will also increase. This means that sonication time greatly affected the exfoliation process.

4.2 FTIR analysis

FTIR analyses can be used to identify the functional group present in the sample after exfoliation. The chemical environment of all Graphene samples at different sonication time has been analysed by FTIR and spectrums of are shown in figure 4.9. All the sample was sonicated at 50% power and centrifuge at 8000 rpm for 1 hr. It was reported that the band $\sim 1475\text{ cm}^{-1}$ and $\sim 1600\text{ cm}^{-1}$ is the spectrum region corresponding to aromatic C=C stretching (Liu et al., 2012). After ultrasonic treatment it was found that all the sample exhibit spectrum attribute to C=C aromatic stretching of 1618 cm^{-1} , 1505.53 cm^{-1} , 1640.49 cm^{-1} and 1507.80 cm^{-1} for 1 hr, 2 hr, 3 hr and 5 hr respectively. From this spectrum it can be observed that how well the samples to absorb light at each wavelength show almost identical for the first 3 sample. But, by prolonged the sonication time to 5 hr, the spectrum start to change and differ from the first 3 samples. So, this suggesting, after 3 hr of sonication time, the graphite start to exfoliate into graphene and therefore the effect of sonication time to the functional group of the nanoparticle can be observed.

This hypothesis can be supported with the peak decreased with a decrease in the thickness of graphene sheets which can be obtained from TEM analysis, the low intensity of the adsorption peak in sample demonstrated that ultrasonic treatment at a long time could increase the exfoliation of graphene solution to the reduced flake size of graphite (Monir et al., 2016). As observed form TEM the exfoliation of graphene in a solvent, with an increasing sonication time, thickness of the sheets is reduced; however, at longer sonication time, it can be reduced to the thickness of the sheets and also affect the quality of graphene for using in several applications (Lee and Rhee, 2014).

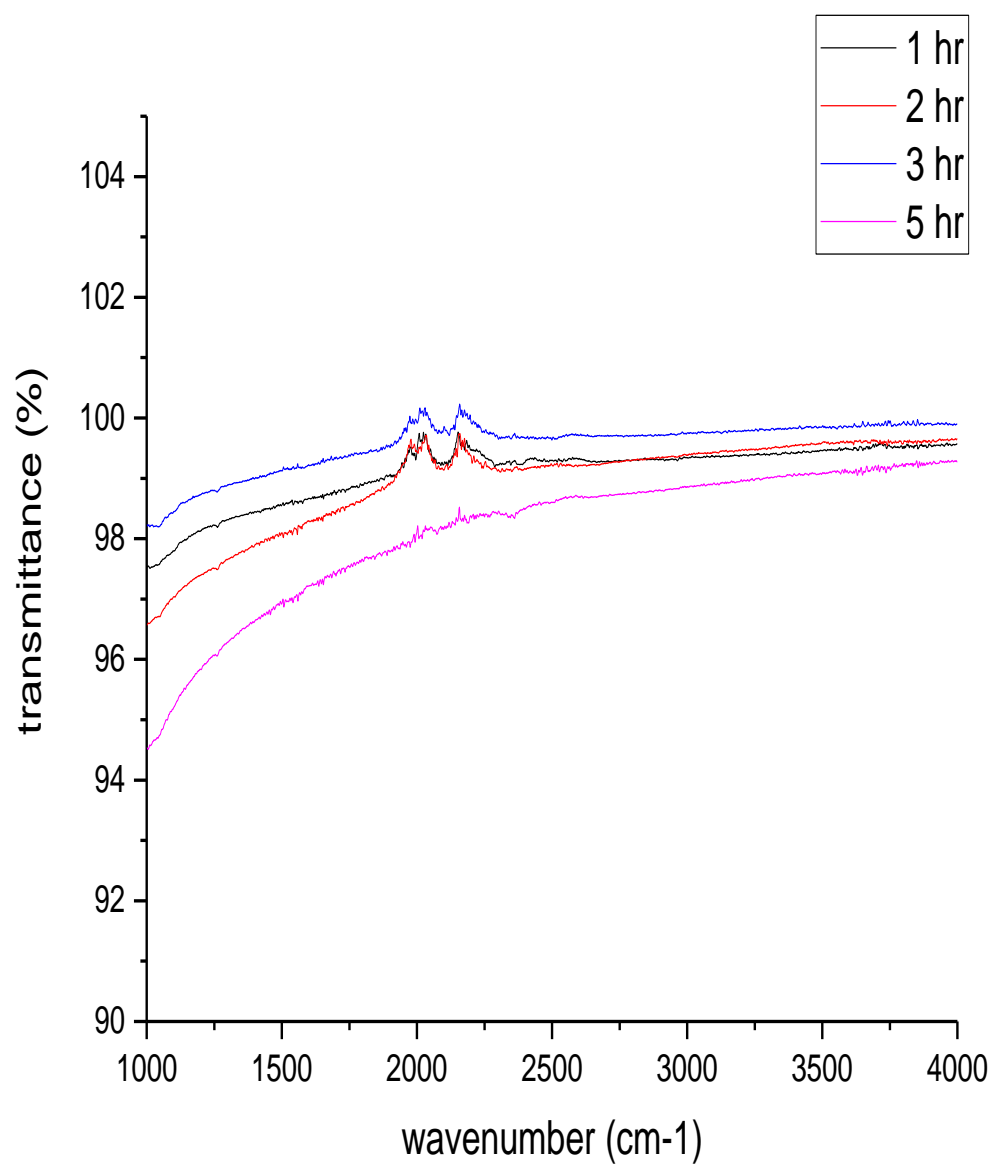


Figure 4.9: FTIR spectrum of samples at different sonication time.

Beside sonication time, other parameter like sonication power and centrifuge speed also can be studied by refereeing FTIR spectrum shown in figure 4.10. All the sample as shown on this spectrum has been sonicated for 2 hr with vary sonication power and centrifuge speed (rpm). From this spectrum it was observed that all the sample exhibit peak value correspond to the C=C aromatic stretch vibration which is 1508.49 cm^{-1} (40%, 5000 rpm), 1623.16 cm^{-1} (50%, 5000 rpm), 1511.18 cm^{-1} (40%, 8000 rpm) and 1505.53 cm^{-1} (50%, 8000rpm). However, by increasing the sonication power from 40% to 50%, the amount of light absorbed by the sample show almost the same, suggesting that sonication power does not influence the functional group of graphene.

On the other hand, by varies the centrifuge speed, there are slightly different on the spectrum that can be observed on figure 4.10. Meaning that, the sample ability to absorb light at each wavelength decreasing as the centrifuge speed decreasing. From this spectrum, low centrifuge speed exhibit low transmittance value indicates increasing or better exfoliation of graphene. This finding different with the UV-Vis analysis suggesting higher centrifuge speed exhibit higher graphene dispersion concentration. Therefore, the effect of centrifuge speed can be seen on this FTIR analysis.

From all the FTIR spectrum, it can be confirm that there are no present of hydroxyl group since the absences of Graphite oxide (GO). Following the work of Varrla et al, it is observed that the spectrum of graphite is deficient of any functional groups except O-H stretching vibrations (3427 cm^{-1}) whereas GO identified the presence of following functional groups. In their work, O-H stretching vibrations (3432 cm^{-1}), CH₂ asymmetric and symmetric stretching vibrations (2924 and 2852 cm^{-1}), C=O stretching vibrations (1725 cm^{-1}), C=C from unoxidized sp² bonds (1627 cm^{-1}), O-H bending deformation (1408 cm^{-1}) and C-O vibrations (1049 cm^{-1}) can be found on the GO spectrum (Varrla et al., 2011). This confirms the presence of hydroxyl, epoxide and carbonyl functional groups in GO.

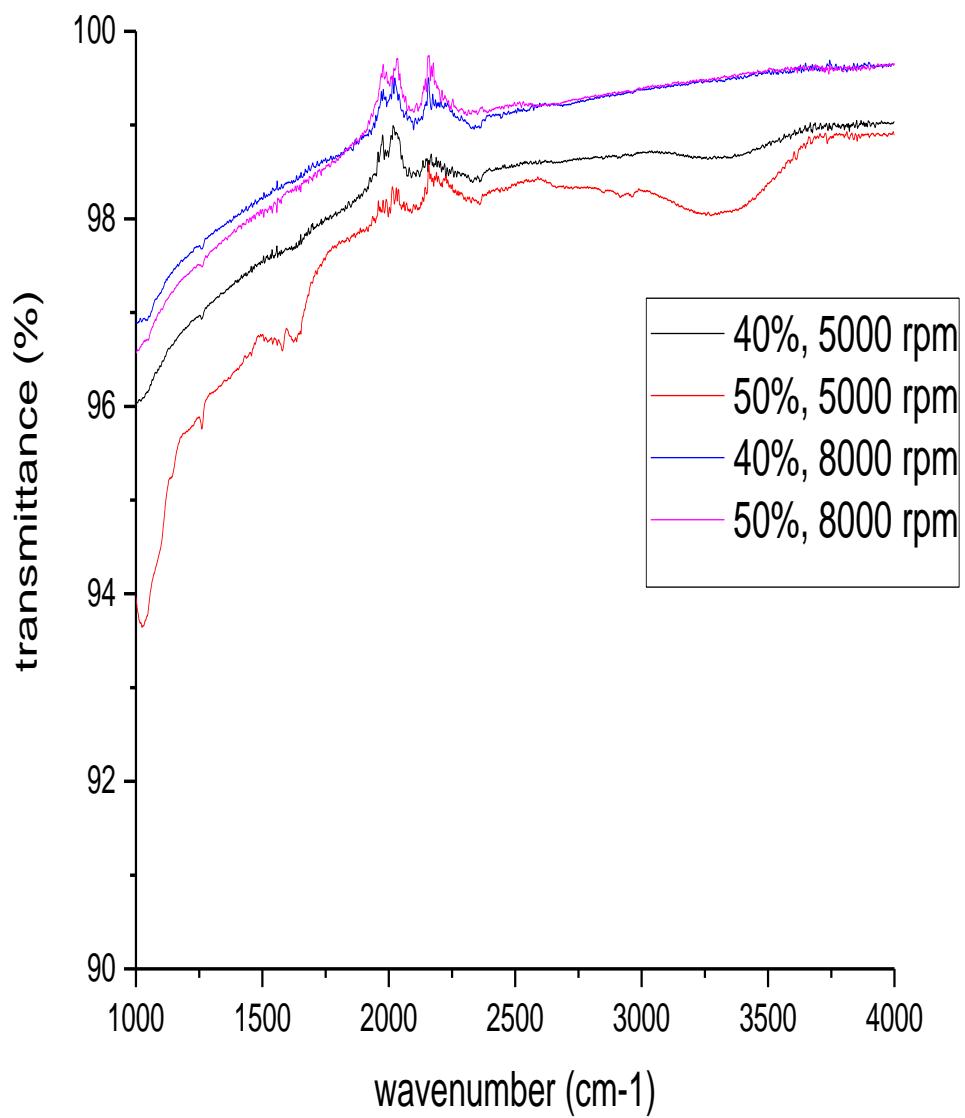


Figure 4.10: FTIR spectrum at different sonication power and centrifuge rate

4.3 TEM Analysis

Electron microscopy enables one to determine the stacking order and the orientation of the graphene layers with respect to each other, as well as determining the size of the sheet (Zan, 2012). This is achieved by randomly moving around the grid and imaging the nanosheets. It is important to image a fair representation of both small and large flakes, with this type of sample; there is a bias to larger flakes due to the fact that small flakes can be difficult to see on the surface of the TEM grid. Therefore, the count of nanosheets is greater for larger than smaller flakes. Once a random selection of nanosheets has been imaged the statistical analysis can be performed. To generate length of the sample, a line is drawn to encompass the longest axis of the nanosheet and were measured.

Figure 4.11 shows a representative TEM image of the graphene sheet in the 1 hr sonication time sample (GZ5). The lateral sizes of the sheet are relatively large, which are ~975 nm. Folded regions can be observed in most of the sheets (yellow arrows point out the folded regions) and primarily located at the edges of the sheet. These prove that defect of the sheet are primarily located at the edges while the basal plane are defect free. The dark colour also shows that the graphene sheet consist of multi-layered. It can be observed that large graphene sheets with several small embedded pieces in it. These indicates that 1 hr of sonication time still does not effectively break the Van der Waals bond that present between graphite`s structure. Therefore, for 1 hour sonicated time, the graphene crystallite are present in agglomerated form with multiple-layered which can be considered as low quality graphene.

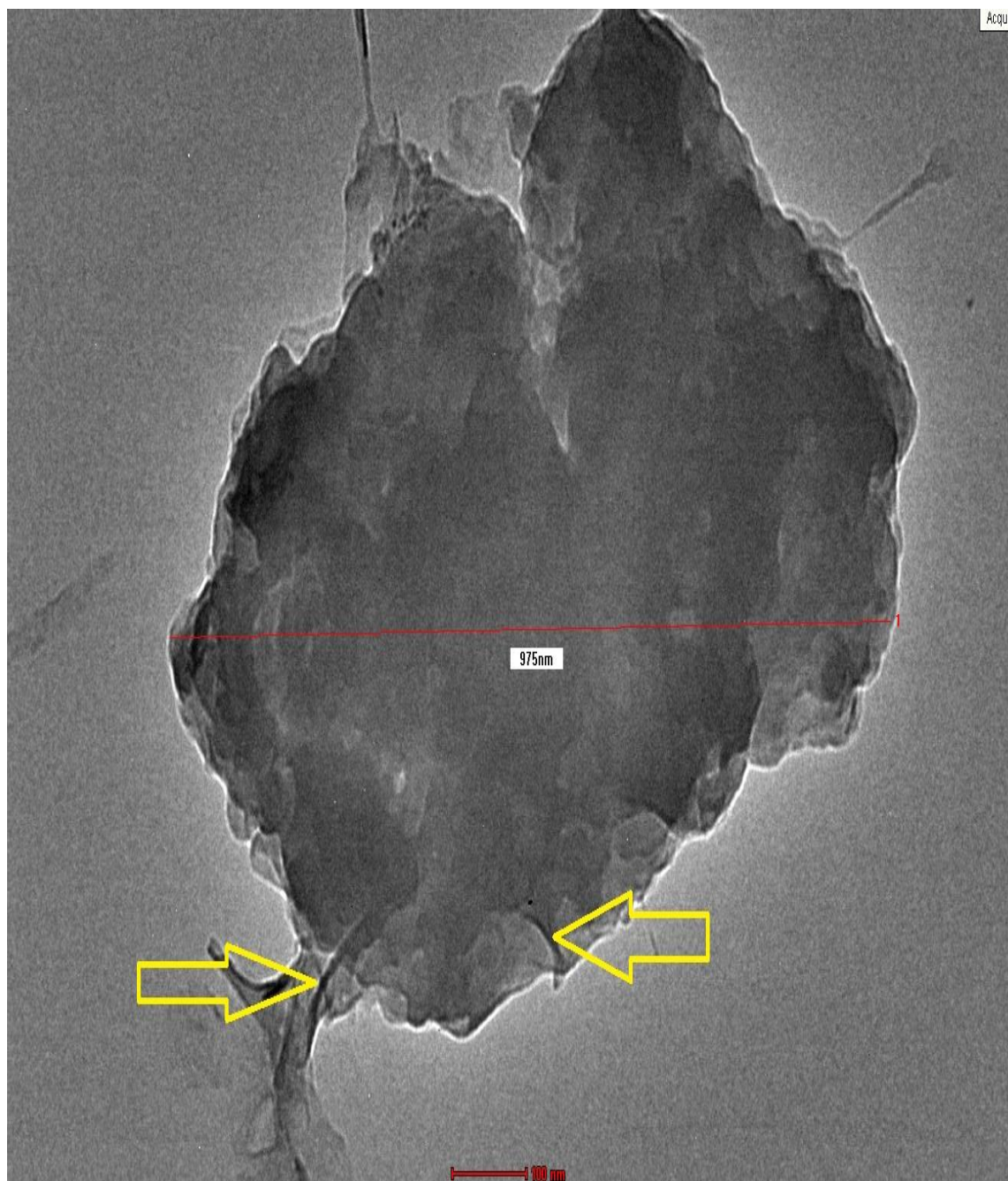


Figure 4.11: TEM image of graphene sheet deposited from 1 hr sonication time sample (scale: 100nm). Yellow arrows show the folded regions.

By prolonged the sonication time to 2 hr, the size of the sheet start to decrease and were measured around 754 nm as shown in figure 4.12. This is because as the time increase, more energy can be supplied to aid the exfoliation process. Thus, resulting a better exfoliation of graphene (Guittonneau et al., 2010). Compare to 1 hr sonication time, the number of layer on 2 hr of sonication time start to decrease judging from the colour of the particle. However, the number of layer deposited from this sample are still too many.

Many research paper highlighted that the folded edge of a graphene-like sheet can provides a clear TEM signature of the number of layers and therefore of the thickness. When the c-planes of a folded graphene sheet are locally parallel to the electron beam, dark lines spaced appear, one for each layer (Meyer et al., 2007). The folded edge of a bi-layer graphene exhibits two dark lines, like double-walled nanotubes and a monolayer graphene shows only one dark line, like single-walled nanotubes. Therefore, from figure 4.12, it can observed that 2 hr of sonication time still exfoliate graphene into multiple-layered but better compared to in the 1 hr of sonication sample

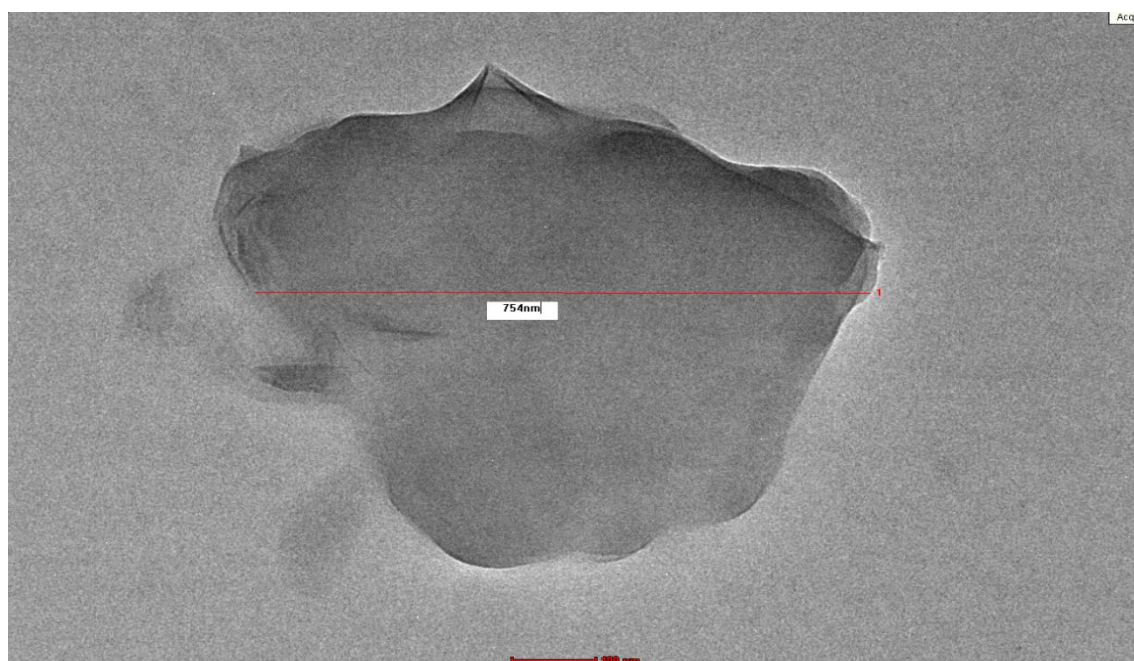


Figure 4.12: TEM images for 2 hr sonication time sample. The graphene particle present in agglomerated form with multiple layers (scale: 100nm).

It is clear that the graphene sheet produces on 2 hr sonication time still does not meet the requirement as high quality graphene, since high quality graphene sheet compose of bi-layer or mono-layer with a flat surface (Henrich et al., 2007). When increased the sonication time to 5 hr (GZ7), the result shows graphene exfoliate into stack of several single graphene layer which can be seen in figure 4.13. The size of the sheets also can be seen dramatically reduced and measured around 206 nm. These suggesting that 5 hr sonication time still does not able to achieve complete, but can partially exfoliated graphene (Hu and Chen, 2010). However from TEM image in figure 4.14, there are evidence that some of the sheet observed in the survey were clearly monolayers of graphene. The results indicated that the resultant graphene sheets are dispersion of single and few layer graphene sheets, which were well exfoliated without significant structural defects, so this process could be scaled up successfully.

In this finding, it can be conclude that graphene crystallite are present in agglomerated form (multilayer) in GZ5. By prolonged the sonication time to 2 hr (GZ3 and GZ4), the graphite crystallite can be reduced into few layer. However, better exfoliation of graphene sheets with several layer can be observed in GZ7. This indicates that a particular sonication time is required for the exfoliation of graphene in particular solvent (tea polyphenol in this case) (Monir et al., 2016). Therefore, 1 hr sonication does not effectively separate the graphite particles into few-layer of graphene, 2 hr sonication can separate some portion of the graphite particles, and 5 hr sonication can exfoliate better with few-layered of graphene. This result indicate that sonication time can somehow influenced the morphology of exfoliate graphene sheet. Thus, by increasing the sonication time, the graphene sheets size tend to be reduced into smaller with consist of less graphene layer.

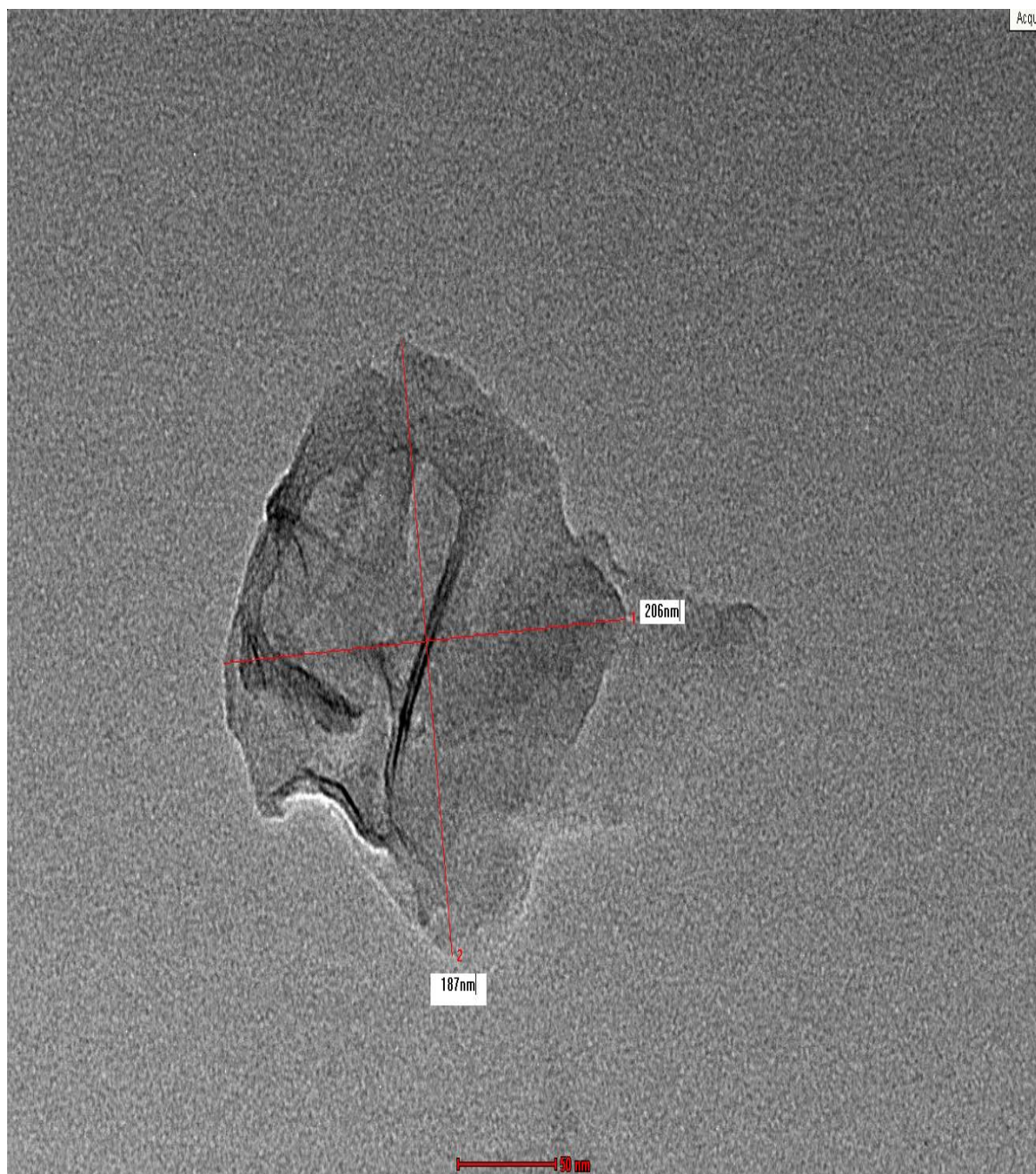


Figure 4.13: TEM image for 5 hr sonication time (scale: 50nm). Partially exfoliated graphite with the stack of several single layer graphite (graphene).

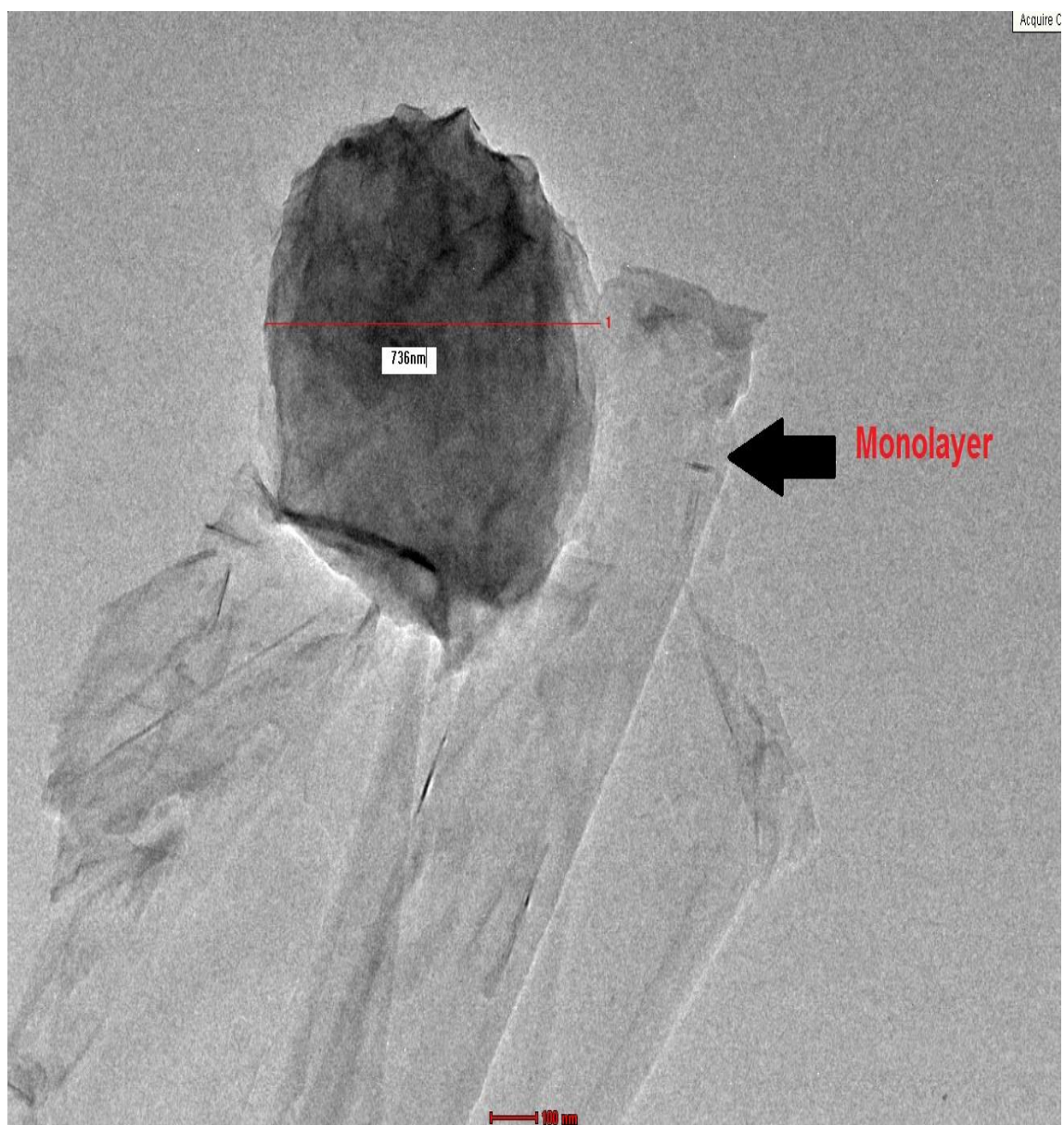


Figure 4.14: TEM image for 5 hr sonication time (scale: 100nm). Monolayer and very large sheet can be observed.

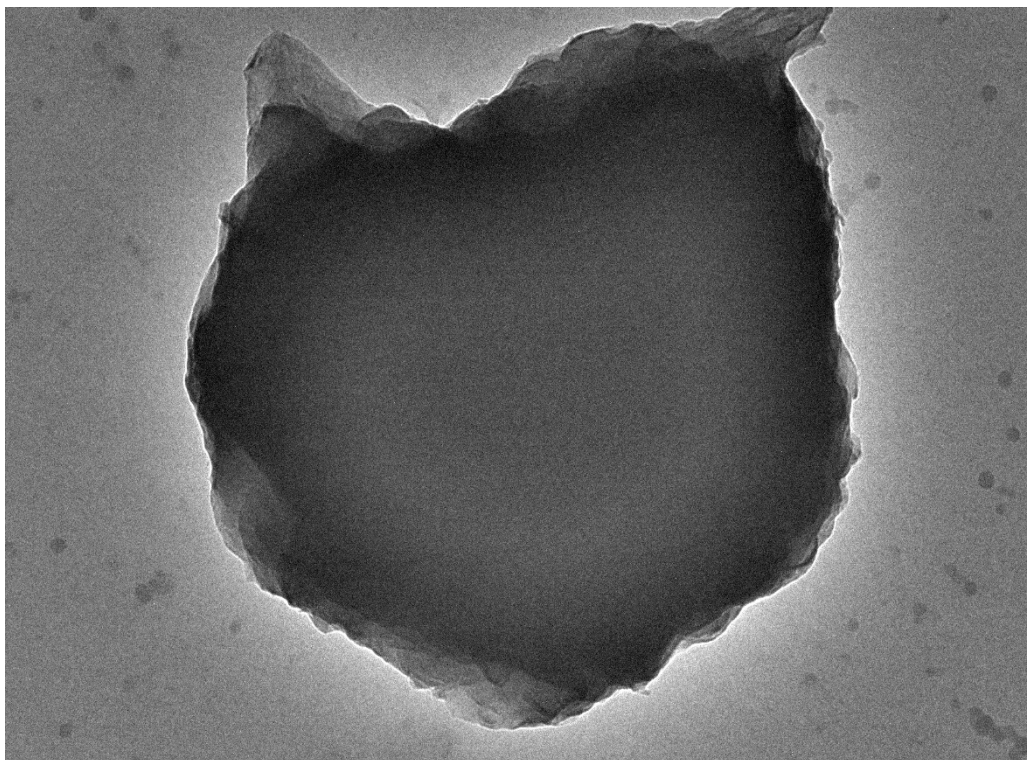
Effect of sonication time on morphology analysis also can be seen and have been studied by Christian et al. In their work, graphite precursor was obtained by sonicating expanded graphite (EG) in chitosan solutions at different time points (0 h-control, 2, 4, 6 and 8 h). After the sonication step, the solutions were centrifuged at 5000 rpm for 20 min in order to collect supernatant solution containing the polymer and the precursor. The EG-chitosan films were then prepared using the solvent evaporation technique. For each time point, film forming solutions were then poured on Teflon plates and left to dry for 24 h at 25 °C, until the total evaporation of the solvent.

They find that, the morphology of EG-chitosan composites, evaluated by TEM analysis revealed a large quantity of flakes with different structures varying the sonication time. In particular, TEM image of composites after 2 h of sonication shows a small quantity of monolayer EG flakes. A larger quantity of flakes with few layers (including some bilayers and tri-layers) can be observed when the sonication time is increased. Furthermore, a transparent sheet-like structure can be found in their work indicating the presence of monolayers. They observed that the selected sheet could be arranged in a single crystal and the obtained products include monolayer graphene sheets (Gayathri et al., 2014). In general, they conclude that the majority of these few-layer flakes had lateral dimensions of $\sim 1 \mu\text{m}$. Thicker flakes, with more than a few graphene layers per flake, were larger, ranging up to $3 \mu\text{m}$ in diameter (Christian et al., 2015).

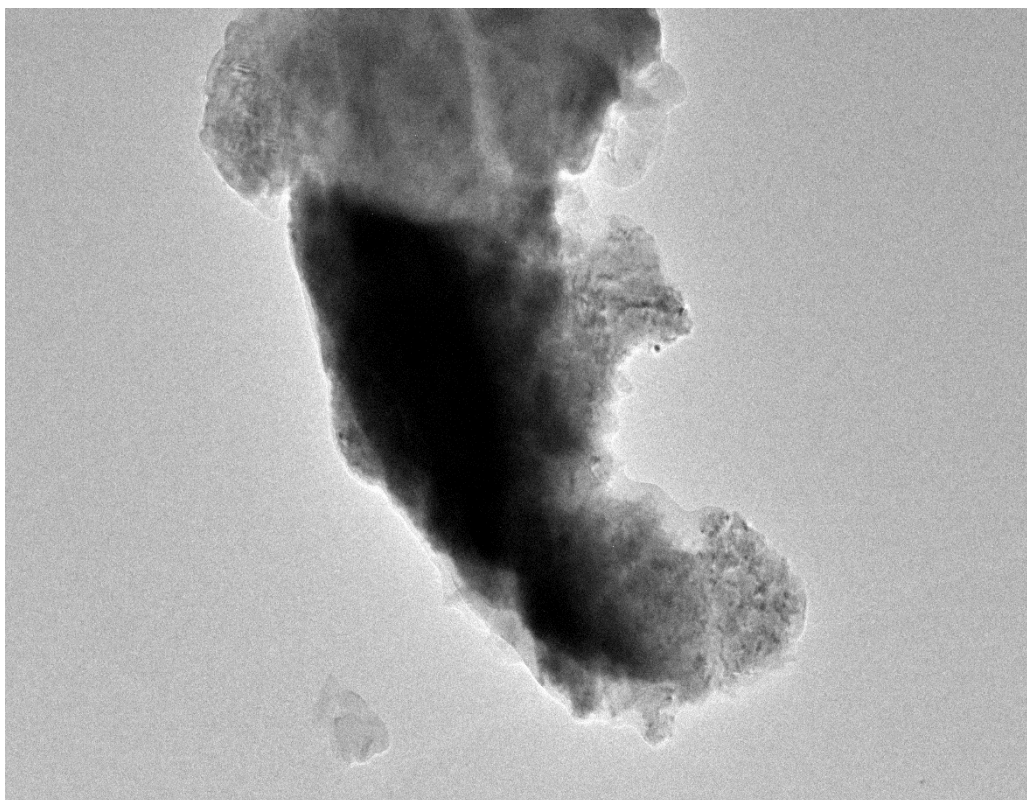
By comparing these previous work, it can find that sample with chitosan solution show better exfoliation compare to Tea Polyphenol. This can be proved that in chitosan solution, TEM image of composites after 2 h of sonication shows a small quantity of monolayer EG flakes. While TEM image for sample sonicated in Tea Polyphenol show only multi-layered graphene.

To study the effect of sonication power on morphology of exfoliated graphene, figure 4.15 (a) show the TEM images for sample 40% sonication power while (b) represent for sample 50% sonication power. Both of sample have undergo sonication treatment for 2 hr and centrifuge at 8000 rpm for 1 hr. Theoretically, 50% sonication power should have better result in term of number of layer since the energy supplied is much higher compared to 40%. Which more energy being supplied, the C-C bond can be effectively destroyed in order to achieve complete exfoliation (Zhou et al., 2008). This hypothesis can be supported by the TEM image which show that sample for 40% sonication power contain more number of layer compared to sample 50 % sonication power. By judging the crystallite colour which are darker in sample in figure 4. 15 (a) compared to (b) which are more transparent. Thus, it is clear that increasing sonication power result in decreasing number of layer in the crystallite. Besides that, the size also can be observed decreasing when increases the sonication power. Therefore, the effect of sonication power can be clearly seen in the morphology analysis.

Generally, study of the effect of the sonication energy on exfoliation of graphene have been studied and can be find in many research paper. Previously, from the work by Rakhee et al, the effect of sonication energy on exfoliation of graphene have been studied by comparing the result deposit from low power sonicator (bath sonicator) and high power probe. In their finding, TEM images that graphene nanosheets exfoliation takes place in bath sonicator consist of number of layers, while TEM images in high power probe shows the less number of graphene nanosheets as compared to the graphene suspension bath sonicated (Rakhee et al., 2014). So this suggesting that, finding in this work shows almost identical to the previous work.



(a)



(b)

Figure 4.15: TEM images for sample (a) 40% sonication power (b) 50% sonication power (both image were taken at 9.6k x resolution).

4.4 XRD Analysis

The structural changes occurring during the conversion of graphite to graphene were studied using X-ray diffraction patterns. Figure 4.16 presents the XRD patterns of exfoliated graphite sonicated at different time.

Based on the work by Vorrada et al., they find that the XRD patterns for pure graphite has a strong and sharp diffraction peak at $2\theta = 26.38^\circ$, corresponding to the highly organized layer structure with an interlayer distance of 0.34 nm along the (002) orientation (Thakur and Karak, 2012). After the chemical oxidation and exfoliation into GO, the (002) peak is shift to lower angle at $2\theta = 10.80^\circ$, indicating an increase in d-spacing from 0.34nm to 0.82 nm. They also highlighted that an increased interlayer distance between consecutive carbon basal planes is attributed to the intercalation of oxygen functional groups and water molecules into carbon layer structure (Achaby et al., 2012). The RGO, on the other hand, they find a new broad peak at $2\theta = 23.50^\circ$, corresponding to the d-spacing of 0.38 nm along the (002) orientation. So they conclude that, these can be explained by the removal of oxygen functional groups, causing a decrease in d-spacing (Vorrada et al., 2013).

In this work the XRD pattern for each sample shown in figure 4.16 and table 4.3, suggesting that 1 hr to 5 hr sonication only resulted partially exfoliated graphene which shown good agreement with the TEM result. This can be proved by sample sonicated at 1 hr exhibit peak related to the periodic lamellar structure of graphite (002) at $2\theta = 26.533^\circ$ with d-spacing of 3.3566 Å and three peaks associated with its in-place crystalline structure at $2\theta = 44.55^\circ, 54.636^\circ, 77.431^\circ$. By prolonged the sonication time to 3 hr, (002) start to shift to $2\theta = 26.493$ with d-spacing of 3.3616 Å. Four additional peaks located at $42.324^\circ, 44.494^\circ, 54.620^\circ, \text{ and } 77.422^\circ$ showed up, suggesting that tea polyphenol had successfully entered the interlayer space of natural graphite, which resulted in a change of the lamellar structure in the c-axis direction and also changes of in-plane crystalline structure due to the interaction with carbon atoms (Ming et al., 2014).

After sonication treatment for 5 hr, the peaks for (002) continue to shift to $2\theta=26.466^\circ$ with d-spacing of 3.3649 Å. Figure 4.16 also reveal that with the increasing sonication time the peak at $2\theta=26^\circ$ become sharper, indicating higher crystallinity of sample. Therefore, it is clear that, 5 hr of sonication time still resulted in partially exfoliation graphene. From this result, although the shifted value for (002) are slightly difference compare to other samples, but it can be used to prove that sample with 5 hr of sonication time result in better exfoliation process.

Compare to the work by Christian et al., by using chitosan solutions as dispersion agent and sonicated at different time. They find that, initially, the intercalated graphite platelets show an intense peak at $2\theta = 26.02^\circ$ (corresponding to $d = 0.336$ nm, attributed to the intercalation of sulfuric acid) and only a shoulder at $2\theta = 26.54^\circ$. After the expansion, XRD analysis on EG shows a reduced intensity of the peak at $2\theta = 26.05^\circ$, resulting from sulfuric acid decomposition, leading to a lower amount of intercalated graphene. But the main point is that, in the case of expanded and sonicated graphite in chitosan (2 hr and 8 hr), the position of the second peak remained roughly the same; on the other hand, the peak at $2\theta = 26.05^\circ$ vanished, as a consequence of a complete disaggregation of intercalated galleries, independently of the time sonication. Therefore, they suggests that the sonication of the EG may lead to an increase of the aspect ratio of the nanofiller, and that the time of sonication does not affect the grade of exfoliation (Christian et al., 2014).

Complete exfoliation also can be seen in the work by Marlinda. So, the different between complete and partial exfoliation of graphene can be studied by comparing these work. In her work, the graphite flakes exhibit the sharp diffraction peak at 26.7° contributed from the highly crystalline of graphene stacks. Whereas, the GO shows the appearance of a new lower intensity peak cantered at 11.1° , corresponds to a d-spacing of 8.29 Å, which is attributed to the (001) reflection of GO. Hence, this result suggests the complete oxidation of graphite (Zhang et al., 2011) and the distance between the carbon sheets is increased due to the insertion of the inter-planar groups. Consequently, she also mention that, the GO sheets' thickness is increased because of the presence of covalently bound oxygen atoms and the displacement of the sp^3 -hybridized carbon atoms above and below the surface of the original graphene sheets (Marlinda, 2012).

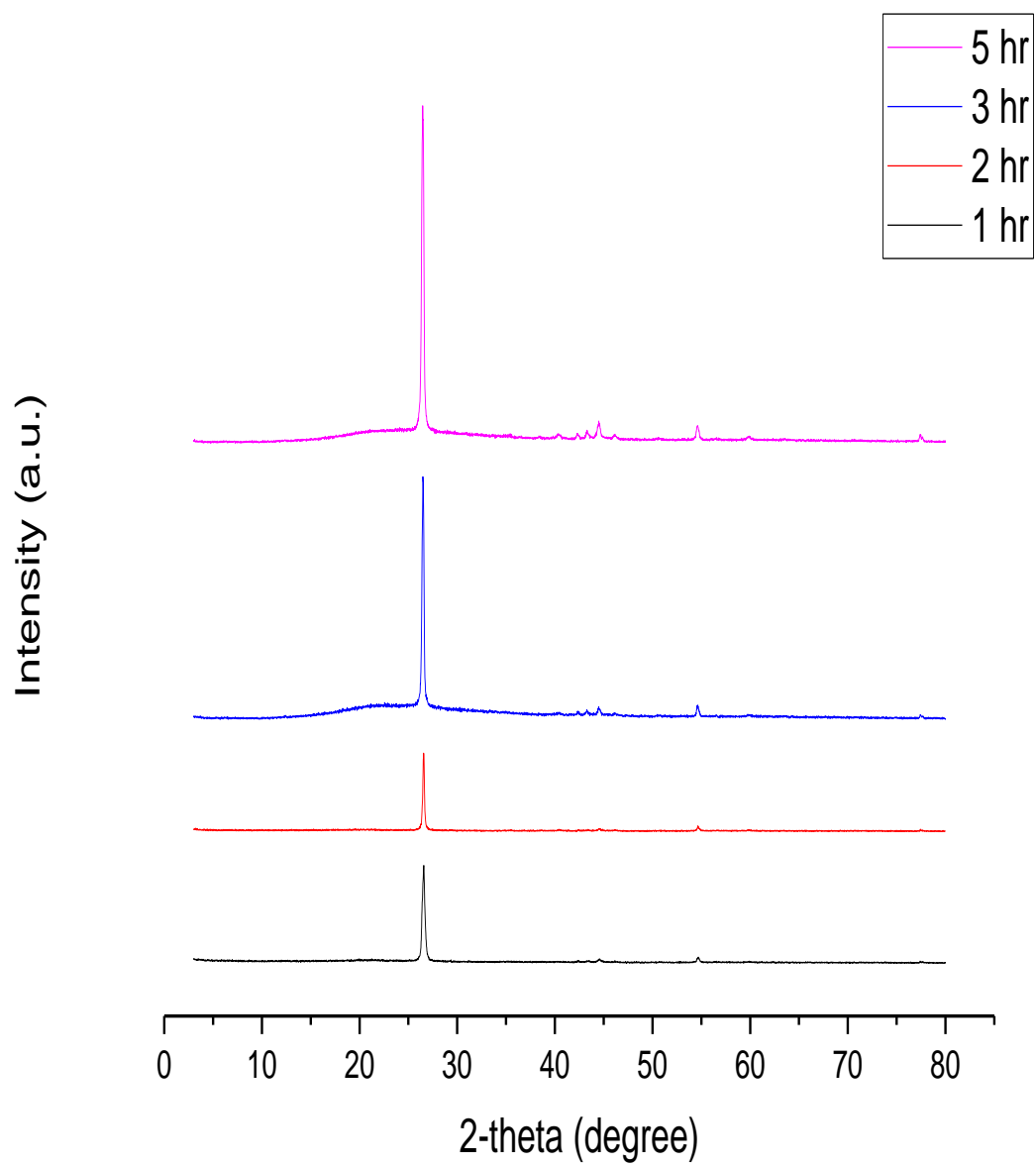


Figure 4.16: XRD pattern of graphite sonicated at different time (hr).

Table 4.3: Peak list summary for samples at different sonication time

Sample	2-theta(deg)	d (ang.)	Phase name
GZ5 (1 hr)	26.533	3.3566	Graphite(0,0,2)
	44.55	2.0319	Graphite(1,0,1)
	54.636	1.6784	Graphite(0,0,4)
	77.431	1.23155	Graphite(1,1,0)
GZ4 (2 hr)	26.552	3.3542	Graphite(0,0,2)
	44.521	2.0334	Graphite(1,0,1)
	54.664	1.6777	Graphite(0,0,4)
	77.473	1.23100	Graphite(1,1,0)
GZ6 (3 hr)	26.493	3.3616	Graphite(0,0,2)
	42.324	2.1337	Graphite(1,0,0)
	44.494	2.0346	Graphite(1,0,1)
	54.620	1.6789	Graphite(0,0,4)
	77.422	1.23168	Graphite(1,1,0)
GZ7 (5 hr)	26.466	3.3649	Graphite(0,0,2)
	42.28	2.136	Graphite(1,0,0)
	44.47	2.0357	Graphite(1,0,1)
	54.573	1.6802	Graphite(0,0,4)
	59.761	1.5462	Graphite(1,0,3)
	77.425	1.23163	Graphite(1,1,0)

XRD also can be used to study the effect of sonication power on the exfoliation graphene. The XRD patterns for samples which are sonicated at different sonication power for 2 hr are shown in figure 4.17 and the peak are summarized in table 4.4. It is observed that 40% sonication power exhibit peak value for graphite (002) at $2\theta = 26.465^\circ$ with d-spacing of 3.3651 Å, while 50% only resulted in $2\theta = 26.552^\circ$ with d-spacing of 3.3542 Å. Meaning that, 40% sonication power deposited better exfoliation graphene. Theoretically, high sonication power should deposited better exfoliation compare to low sonication power since more energy is supplied during exfoliation process. But for this case, at 40% sonication power, the peak for graphite (002) shifted and four additional peak located at 42.248° (1,0,0), 44.443° (1,0,1), 54.526° (0,0,4), and 77.406° (1,1,0) can be observed. Suggesting that TP had successfully entered the interlayer space of natural graphite, which resulted in a change of the lamellar structure in the c-axis direction and also changes of in-plane crystalline structure due to the interaction with carbon atoms (Ming et al., 2014). However, when increasing sonication power to 50% there is a decrease in the intensity and the peak becomes broad in comparison with 40%, which means that the inter planar carbon bonds get broken and the crystalline size of graphite is reduced from 3.3651 Å to 3.3542 Å.

This result completely different compare to others result obtained from different analysis which highlighted that high sonication power exhibit better exfoliation graphene. In TEM analysis alone, it is clear that 50% sonication power can produce smaller graphene sheets with less number of layer compared to 40% sonication power.

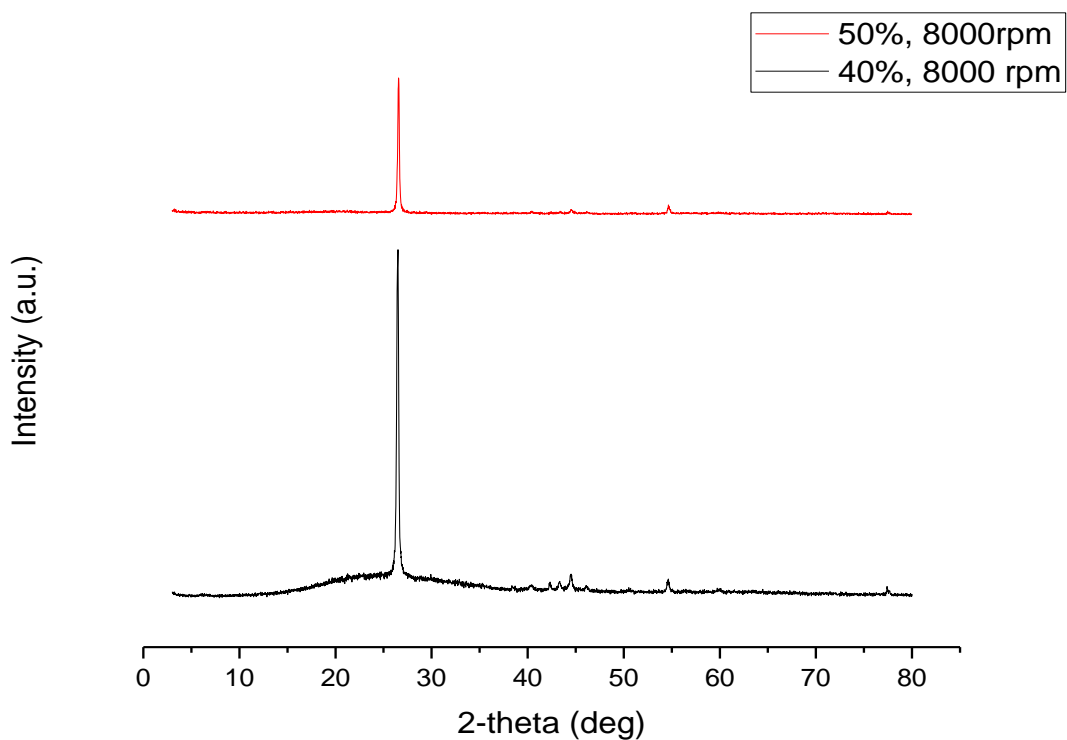


Figure 4.17: XRD pattern of graphite sonicated at different power (%).

Table 4.4: Peak list summary for samples at different sonication power

Sample	2-theta(deg)	d (ang.)	Phase name
40% power (GZ3)	26.465	3.3651	Graphite(0,0,2)
	42.248	2.1374	Graphite(1,0,0)
	44.443	2.0368	Graphite(1,0,1)
	54.526	1.6815	Graphite(0,0,4)
	77.406	1.2319	Graphite(1,1,0)
50% power (GZ4)	26.552	3.3542	Graphite(0,0,2)
	44.521	2.0334	Graphite(1,0,1)
	54.664	1.6777	Graphite(0,0,4)
	77.473	1.23100	Graphite(1,1,0)

CHAPTER 5

CONCLUSION AND RECOMMENDATION

5.1 Conclusion

Liquid-phase exfoliation of bulk graphite is an extremely mild, versatile and potentially up-scalable approach to obtain high quality graphene. In order to achieve that, processing parameters must have to be studied thoroughly for better understanding. In this present work, the graphene nanocomposites were successfully synthesized in LPE method by using Tea Polyphenol as dispersion agent.

The structural properties of nanocomposites were confirmed in the XRD analysis, which all the diffraction peaks of nanocomposites are match with the standard data. From this result, it can be conclude that longer sonication time resulted better exfoliation. This hypothesis also can be supported by TEM analysis, which shows sample sonicated for 5 hr deposit smaller graphene sheets with around 206 nm in diameter with few layer. However, from both analysis, it can be conclude that the graphite only partially exfoliated with the stack of several or tens of single layer graphite. Beside sonication time, TEM also can use to study the effect of sonication power on exfoliation process which show high sonication power exhibit smaller and few layer sheets.

Besides that, UV-vis analysis also can be used to study the effect of professing parameters. It is conclude that, sample sonicated at high power and at longer time give the highest value of graphene dispersion concentration which is 1.0699 mg/ml. But, when manipulating the centrifuge speed (rpm), the graphene dispersion concentration does not show any significant different. This is because, for centrifuged graphene dispersions, the average lateral flake size decreases as the centrifugation rate increases. So it only affect the size of graphene flake.

Therefore, by controlling LPE critical parameter likes sonication power, sonication time and centrifuged speed, graphene can produce at high scale. This is because, from the chemistry point of view, the LPE in the presence of a given solvent molecule with the aid of an additional pre-designed (macro) molecule as an exfoliating agent is a path not only to increase exfoliation yield but also to avoid graphene re-aggregation due to van der Waals attraction, thereby compromising the effort made during exfoliation. Hence, LPE can be proved to be a suitable convenient approach for massive production of graphene.

5.2 Recommendation

Liquid-phase exfoliation is appealing for the preparation of stable inks that can be processed in thin films and composite materials; in this regard more research is needed to control on-demand the number of layers and lateral size. In spite of the vital prospect of mechanical exfoliation, several issues are still required for continuous attention. Technical factors such as frequency, vessel geometry, sonication source distribution, etc., should attract interests for optimizing exfoliation efficiency and scaling up production (Ming et al., 2012). Besides that, the parameter also must be in wide range in order to make sure the process parameters studied systematically. In addition, future challenges should also focus on the problems with uncontrollable defects, random size, and random layer number of graphene in mechanical exfoliation.

REFERENCES

- Artur Ciesielskia and Paolo Samorì. (2014). Graphene via sonication assisted liquid-phase exfoliation. *Chem. Soc. Rev.* **43**: 381-398
- Ashcroft N. W and Mermin N. D. (1976). Solid state physics. New York: Holt, Rinehart and Winston.
- Bae S., Kim H, Lee Y., Xu X., Park J., Zheng Y., Balakrishnan J., Lei T., Kim H. R., Song Y., Kim J., Kim K. S., Özyilmaz B., Ahn J., Hong B. H. and Iijima S. (2010). Roll-to-roll production of 30-inch graphene films for transparent electrodes. *Nature Nanotechnology.* **5**: 574-578.
- Bolotin K. I., Sikes K. J., Jiang Z., Klima M., Fudenberg G., Hone J., and Stormer H. L. (2008). Ultrahigh electron mobility in suspended graphene. *Solid State Communications.* **146**: 351-355.
- Bourlinos A. B., Georgakilas V., Zboril R., Steriotis T. A. and Stubos A. K. (2009). Liquid-phase exfoliation of graphite towards solubilized graphenes. *Small.* **5**: 1841–1845.
- Bracamonte M. V., Lacconi G. I., Urreta S., Foa Torres L. E. F. (2014). On the nature of defects in liquid-phase exfoliated graphene. *Journal of Physical Chemistry C.* **118**: 15455-15459.
- Brodie B. C. (1859). On the Atomic Weight of Graphite. *Philosophical Transactions of the Royal Society of London.* **149**: 249-259.
- Choi W., Lahiri I., Seelaboyina R. and Kang Y. S. (2010). Synthesis of Graphene and Its Applications: A Review. *Critical Reviews in Solid State and Materials Sciences.* **35**: 52-71.
- Christian Demitri, Anna Moscatello, Antonella Giuri , Maria Grazia Raucci and Carola Esposito Corcione. (2015). Preparation and Characterization of EG-Chitosan Nanocomposites via Direct Exfoliation: A Green Methodology. *Polymers.* **7**: 2584–2594.

Chu H. Y. (2011). Development of Solution-Processed Methods for Graphene Synthesis and Device Fabrication. *Georgia Institute of Technology*.

Chugh S., Mehta R., Lu N., Dios F. D., Kim M. J. and Chen Z. (2015). Comparison of graphene growth on arbitrary non-catalytic substrates using low-temperature PECVD. *Carbon*. **93**: 393-399.

Cummins G. and Desmulliez M. P. Y. (2012). Inkjet printing of conductive materials: a review. *Circuit World*. **38**: 193 – 213.

Dikin D. A., Stankovich S., Zimney E. J., Piner R. D., Dommett G. H. B., Evmenenko G., Nguyen S. T. and Ruoff R. S. (2007). Preparation and characterization of graphene oxide paper. *Nature*. **448**: 457-460.

Eda G., Fanchini G., and Chhowalla M. (2008). Large-area ultrathin films of reduced graphene oxide as a transparent and flexible electronic material. *Nat Nano*. **3**:270-274.

El Achaby, Arrakhiz F. Z., Vaudreuil S., Essassi E. M., and Qaiss A. (2012). Piezoelectric β -polymorph formation and properties enhancement in graphene oxide—PVDF nanocomposite films. *Applied Surface Science*. **258**: 7668–7677.

Ferrari A. C. (2007). Raman spectroscopy of graphene and graphite: Disorder, electron–phonon coupling, doping and nonadiabatic effects. *Solid State Communications*. **143**: 47-57.

Flint E. B. and Suslick K. S. (1991). The temperature of cavitation. *Science*. **253**: 1397-1399.

Frank I. W., Tanenbaum D. M., Van der Zande A. M. and McEuen P. L. (2007). Mechanical properties of suspended graphene sheets. *J. Vac. Sci. Technol. B*. **25**: 2558–2561

Gayathri S., Jayabal P., Kottaisamy M. and Ramakrishnan, V. (2014). Synthesis of few layer graphene by direct exfoliation of graphite and a Raman spectroscopic study. *Aip Adv.* **4**: 27116.

Guittonneau F., Abdelouas A., Grambow B., Huclier S. (2010). The effect of high power ultrasound on an aqueous suspension of graphite. *Ultrasonics sonochemistry* **17**. **2**: 391-398.

Gong L., Young R. J., Kinloch I. A., Haigh S. J., Warner J. H., Hinks J. A., and Novoselov K. S. (2013). Reversible Loss of Bernal Stacking during the Deformation of Few-Layer Graphene in Nanocomposites. *ACS Nano*. **7**: 7287-7294.

Henrich F., Krupke R., Arnold K., Rojas Stütz J. A., Lebedkin S., Koch T., and Kappes M. M. (2007). The Mechanism of Cavitation-Induced Scission of Single-Walled Carbon Nanotubes. *The Journal of Physical Chemistry B*. **111**: 1932-1937.

Hernandez Y., Nicolosi V., Lotya M., Blighe F. M., Sun Z., De S., and Coleman, J. N. (2008). High-yield production of graphene by liquid-phase exfoliation of graphite. *Nat Nano*. **3**: 563-568.

Huawen Hu and Guohua Chen. (2010). Electrochemically modified graphite nanosheets and their nanocomposite films with poly(vinyl alcohol). *Polymer composites*. **31**: 1770-1775

Hummers Jr W. S. and Offeman R. E. (1958). Preparation of Graphitic Oxide. *J. Am. Chem. Soc.* **80**: 1339–1339

Israelachvili J. N. (2011). Intermolecular and surface forces. *Academic press*. **3**.

Jalili N. and Laxminarayana K. (2004). A review of atomic force microscopy imaging systems: application to molecular metrology and biological sciences. *Mechatronics*. **8**: 907-945.

Jungrok K., Jihoon S., Hyun K. J., Soo H. K. and Hyung W. L. (2012). The effect of various parameters for few-layered graphene synthesis using methane and acetylene. *Journal of Ceramic Processing Research*. **13**: 42-46

Kashyap S, Mishra S and Behera S.K. (2014). Aqueous Colloidal Stability of Graphene Oxide and Chemically Converted Graphene. *Journal of Nanoparticles*. **2014**: 640281

Khan U., Porwal H., O'Neill A., Nawaz K., May P., and Coleman, J. N. (2011). Solvent-Exfoliated Graphene at Extremely High Concentration. *Langmuir*. **27**: 9077-9082.

Khan U, O'Neill A, Lotya M, De S, and Coleman J.N. (2010). High concentration solvent exfoliation of graphene. *Small*. **7**: 64-71.

Kim J., Kwon S., Cho D., Kang B., Kwon H., Kim Y., Park S. O., Jung G. Y., Shin E., Kim W., Lee H., Ryu G. H, Choi M., Kim T. H., Oh J., Park S., Kwak S. K., Yoon S.W, Byun D., Lee Z., and Lee C. (2015). Direct exfoliation and dispersion of two-dimensional materials in pure water via temperature control. *Nature Communication*. **6**: 8294.

Lavin-Lopez M. P., Valverde J. L., Sanchez-Silva L., and Romero A. (2016). Solvent-Based Exfoliation via Sonication of Graphitic Materials for Graphene Manufacture. *Industrial & Engineering Chemistry Research*. **55**: 845-855.

Lee G. J. and Rhee C. (2014). Enhanced thermal conductivity of nanofluids containing graphene nanoplatelets prepared by ultrasound irradiation. *Journal of Materials Science*. **4**: 1506–1511

Lee H., Some S., Kim Y., Hwang E., and Yoo H. (2012). Binol salt as a completely removable graphene surfactant. *Chem. Comm*. **48**: 7732-7734.

Li D., Muller M. B., Gilje S., Kaner R. B. and Wallace G. G. (2008). Processable aqueous dispersions of graphene nanosheets. *Nature Nanotechnology*. **3**: 101-105.

Li X., Cai W., An J., Kim S., Nah J., Yang D., Piner R., Velamakanni A., Jung I., Tutuc E., Banerjee S.K., Colombo L. and Ruoff R. S. (2009). Large-area synthesis of high-quality and uniform graphene films on copper foils. *Science*. **324**.

Liang S., Shen Z., Yi M., Liu L., Zhang X., Cai C., and Ma S. (2015). Effect of processing parameters on massive production of graphene by jet cavitation. *Journal of Nanoscience and Nanotechnology*. **15**: 2686-2694.

Liu Z., Liu Q., Huang Y., Ma Y., Yin S., Zhang X., Sun W. and Chen Y. (2008). Organic photovoltaic devices based on a novel acceptor material: Graphene. *Adv. Mater.* **20**: 3924-3930

Liu W. W., Wang J. N. and Wang, X. X. (2012). Charging of unfunctionalized graphene in organic solvents. *Nanoscale*. **4**: 425-428.

Lotya M., King P. J., Khan U., De S., and Coleman, J. N. (2010). High-Concentration, Surfactant-Stabilized Graphene Dispersions. *ACS Nano*. **4**: 3155-3162.

Malard L. M., Pimenta M. A., G. Dresselhaus G. and Dresselhaus M. S. (2009). "Raman spectroscopy in graphene," *Phys. Rep.* **473**: 51-87.

Marcano D. C., Kosynkin D. V., Berlin J. M., Sinitskii A., Sun Z., Slesarev A., Alemany L. B., Lu W. and Tour J. M. (2010). *ACS Nano*. **4**: 8.

Marlinda bt Rahman, (2012). Efficient preparation of graphene/zinc oxide nanocomposites. *Thesis of Universiti Malaya*. 78-80.

Meyer J. C., Geim A. K., Katsnelson M. I., Novoselov K. S., Booth T. J. and Roth S. (2007). The structure of suspended graphene sheets. *Nature*. **446**: 60-63.

Min Yi and Zhigang Shen. (2013). A review on mechanical exfoliation for scalable production of graphene. *Journal of Materials Chemistry A*. **3**: 11700-11715.

Ming Zhou, Tian Tian, Xuanfu Li, Xudong Sun, Juan Zhang, Ping Cui, Jie Tang, and Lu-Chang Qin. (2014). Production of Graphene by Liquid-Phase Exfoliation of Intercalated Graphite. *Int. J. Electrochem. Sci.* **9**: 810 - 820.

Monir Noroozi, Azmi Zakaria, Shahidan Radiman and Zaidan Abdul Wahab. (2016). Environmental Synthesis of Few Layers Graphene Sheets Using Ultrasonic Exfoliation with Enhanced Electrical and Thermal Properties. *PLOS ONE*. **4**: e0152699.

Moser J., Barreiro A., and Bachtold A. (2007). Current-induced cleaning of graphene Moser. *Applied Physics Letters*. **91**: 163513

Misik V and Riesz P. (1996). Peroxyl radical formation in aqueous solutions of N,N-dimethylformamide, N-methylformamide, and dimethylsulfoxide by ultrasound: implications for sonosensitized cell killing. *Free Radic Biol Med*. **20**: 129-138.

Nicolosi V., Chhowalla M., Kanatzidis M. G., Strano M. S., and Coleman, J. N. (2013). Liquid Exfoliation of Layered Materials. *Science*. **340**: 6139.

Nikitin Y. A. and Pyatkovskii M. L. (1997). Formation and Properties of Materials Based on Thermally Expanded Graphite. *Powder Metallurgy and Metal Ceramics*. **36**.

Novoselov K. S., Geim A. K., Morozov S. V., Jiang D., Zhang Y., Dubonos S. V., Grigoriava I. V., and Firsov A. A. (2004). Electric Field Effect in Atomically Thin Carbon Films. *Science*. **306**: 666–669.

Prawer S. and Nemanich, R. J. (2004). Philosophical Transactions: Mathematical, Physical and Engineering. *Sciences* **362**: 2537-2565.

Pu N. W., Wang C. A., Liu Y. M., Sung Y., Wang D. S. and Ger M. D. (2012). Dispersion of graphene in aqueous solutions with different types of surfactants and the production of graphene films by spray or drop coating. *Journal of the Taiwan Institute of Chemical Engineers*. **43**: 140-146.

Quintana M., Grzelczak M., Spyrou K., Kooi B., Bals S., Van T., Gustaaf R. P., and Prato M. (2012). Production of large graphene sheets by exfoliation of graphite under high power ultrasound in the presence of tiopronin. *Chem. Commun.* **48**: 12159–12161.

Rakhee Durgea, R. V. Kshirsagara, Pankaj Tambeeb. (2014). Effect of sonication energy on the yield of graphene nanosheets by liquid-phase exfoliation of graphite. *Procedia Engineering.* **97**:1457 – 1465

Rekha Narayan and Sang Ouk Kim. (2015). Surfactant mediated liquid phase exfoliation of graphene. *Nano Convergence.* **2**: 15-20

Rod Ruoff S. (2008). Graphene: Calling all chemists. *Nature Nanotechnology.* **3**: 10 – 11.

Ruoff R. S. and Park S. (2009). Chemical methods for the production of graphenes. *Nature Nanotechnology.* **4**: 217-224.

Ruan G., Sun Z., Peng Z. and Tour J.M. (2011) “Growth of Graphene from Food, Insects, and Waste”. *ACS Nano.* **5**: 7601-7607.

Shuai Wang, Min Yi, Shuaishuai Liang, Zhigang Shen, Xiaojing Zhang and Shulin Ma. (2016). The effect of surfactants and their concentrations on the liquid-exfoliation of graphene. *RSC Advances.* **6**: 56705 – 56710

Somani, Prakash R., Savita P., Umeno and Masayoshi. (2006). Planer nano-graphenes from camphor by CVD. *Chemical Physics Letters.* **430**: 56-59.

Stankovich S., Dikin D. A., Piner R. D., Kohlhaas K. A., Kleinhammes A., Jia Y., and Ruoff R. S. (2007). Synthesis of graphene-based nanosheets via chemical reduction of exfoliated graphite oxide. *Carbon.* **45**: 1558-1565.

Tan Y. Y. Tan L. W., Jayawardena K., Anguita J. V., Carey J. D. and Silva S. R. P. (2011). Field effect in chemical vapour deposited graphene incorporating a polymeric gate dielectric. *Synthetic Metal.* **161**: 2249-2252.

Thakur S. and Karak N. (2012). Green reduction of graphene oxide by aqueous phytoextracts. *Carbon*. **50**: 5331–5339.

Umar Khan, Jonathan Coleman and Harshit Porwal. (2012). Size selection of dispersed, exfoliated graphene flakes by controlled centrifugation. *Carbon*. **50**: 470-475.

Uran S., Alhani A., and Silva C. (2017). Study of ultraviolet-visible light absorbance of exfoliated graphite forms. *AIP Advances*. **7**: 035323

Vandana Sharma, Avesh Garg, and Suresh Chander Sood. (2015). Graphene Synthesis via Exfoliation of Graphite by Ultrasonication. *International Journal of Engineering Trends and Technology (IJETT)*. **26**: 38-42.

Varrla Eswaraiah, Sasidharannair Sasikaladevi Jyothirmayee Aravind and Sundara Ramaprabhu. (2011). Top down method for Synthesis of Highly Conducting Graphene by Exfoliation of Graphite Oxide using Focused Solar Radiation. *J. Mater. Chem.* **21**: 17094.

Vorrada Loryuenyong, Krit Totepvimarn, Passakorn Eimburanaprat, Wanchai Boonchompoo, and Achanai Buasri. (2013). Preparation and Characterization of Reduced Graphene Oxide Sheets via Water-Based Exfoliation and Reduction Methods. *Advances in Materials Science and Engineering*. 1-5.

Wallace P. R. (1947). Erratum: The Band Theory of Graphite. *Physical Review*. **71**: 622.

Watson K. D. (2001). Svedberg, Theodor *eLS*: John Wiley & Sons, Ltd.

Williams D. B. and Carter C. B. (2009). *Transmission Electron Microscopy*. USA: Springer.

Xu C., Wang X. and Zhu J. (2008). Graphene metal particle nanocomposites. *J. Phys. Chem. C*. **112**: 19841-19845.

Yu Q., Lian J., Siriponglert S., Li H., Chen Y. P. and Pei S. S. (2008). Graphene segregated on Ni surfaces and transferred to insulators. *Applied Physics Letters* 2008. **96**: 113103.

Zan, R. (2012). Microscopy and spectroscopy of graphene: Atomic scale structure and interaction with foreign atom species. *Manchester: PhD Thesis, University of Manchester, School of Physics and Astronomy.*

Zhang S., Shao Y., Liao H., Engelhard M. H., Yin G., and Lin Y. (2011). Polyelectrolyte-Induced Reduction of Exfoliated Graphite Oxide: A Facile Route to Synthesis of Soluble Graphene Nanosheets. *ACS Nano*. **5**: 1785-1791.

Zhou S. Y., Seigel D. A., Federov A. V., Gabaly F. and Schmid A. K. (2008). Origin of the energy bandgap in epitaxial graphene. *Nature Materials*. **7**: 259–260

APPENDIX

CALCULATION OF CONCENTRATION OF GRAPHENE DISPERSION

The calculation of concentration of graphene dispersion was done as follow Beer-Lambert law.

$$A = \varepsilon CL$$

Rearrange,

$$C = \frac{A}{\varepsilon L}$$

Where

$A = \text{absorbance}$

$\varepsilon = \text{molar absorptivity} \left(\frac{\text{ml}}{\text{mg} \cdot \text{m}} \right)$

$L = \text{length of solution of light passed through (m)}$

GZ1,

$$\begin{aligned} C &= \frac{1.42}{1002 \frac{\text{ml}}{\text{mg} \cdot \text{m}} \times 0.01 \text{m}} \\ &= 0.1417 \frac{\text{mg}}{\text{ml}} \end{aligned}$$

GZ2,

$$\begin{aligned} C &= \frac{2.28}{1002 \frac{\text{ml}}{\text{mg} \cdot \text{m}} \times 0.01 \text{m}} \\ &= 0.2275 \frac{\text{mg}}{\text{ml}} \end{aligned}$$

GZ3,

$$\begin{aligned} C &= \frac{1.23}{1002 \frac{ml}{mg \cdot m} \times 0.01m} \\ &= 0.1228 \frac{mg}{ml} \end{aligned}$$

GZ4,

$$\begin{aligned} C &= \frac{2.72}{1002 \frac{ml}{mg \cdot m} \times 0.01m} \\ &= 0.2715 \frac{mg}{ml} \end{aligned}$$

GZ5,

$$\begin{aligned} C &= \frac{2.34}{1002 \frac{ml}{mg \cdot m} \times 0.01m} \\ &= 0.2335 \frac{mg}{ml} \end{aligned}$$

GZ6,

$$\begin{aligned} C &= \frac{4.04}{1002 \frac{ml}{mg \cdot m} \times 0.01m} \\ &= 0.4032 \frac{mg}{ml} \end{aligned}$$

GZ7,

$$\begin{aligned} C &= \frac{10.72}{1002 \frac{ml}{mg \cdot m} \times 0.01m} \\ &= 1.0699 \frac{mg}{ml} \end{aligned}$$